Assessing the thermodynamic behavior of bunkering compressed hydrogen for inland cargo vessels

Master Thesis

R.S. Rademaker

2023.MME.8892

TU Delft

1

[1]Title page image source: [1]

Assessing the thermodynamic behavior of bunkering compressed hydrogen for inland cargo vessels

Master Thesis

by

R.S. Rademaker

In partial fulfillment of the requirements for the degree of Master of Science
at the Delft University of Technology,

Student number:	4483065	
Project duration:	May 2023 – Jan 2024	
Thesis committee:	Prof. dr. ir. H. Polinder,	TU Delft, supervisor
	Ir. N.H. Goselink	TU Delft, daily supervisor
	Ir. E.S. van Rheenen	TU Delft, daily supervisor
	dr. Ir. M. Godjevac,	Future Proof Shipping

TU Delft

Preface

In a year where I walked the *Nijmeegse Vierdaagse* and started attending salsa classes I couldn't imagine there would be a greater challenge, but yet there was: this very graduation project. What a beautiful challenge this is.

Abstract

A new simulation tool has been developed to provide insights into the refueling process of hydrogen. The tool is based on existing models, including a 0D gas model and a 1D wall model, which have been refined to assist companies like Future Proof Shipping, which rely on compressed hydrogen tanks.

Although the model is still subject to changes and not fully reproducible during the validation process, it has accurately computed the temperature evolution for large tanks ranging from 1500-2100L. Based on this evolution, it is recommended to maintain the inlet temperature of hydrogen at -20°C or lower.

Furthermore, it is suggested that Future Proof Shipping should consider using a type 3 hydrogen tank, which features an aluminum liner and better heat conductivity. This results in more efficient heat conduction away from the hydrogen.

Contents

Nomenclature

Alphabetical symbols

$\dot{m}_{ent}$ Entrainment mass flow rate $[kg/s]$

$\dot{m}_{gas}$ Mass flow rate of the gas in the tank $[kg/s]$

a constant representing the inter-molecular attraction forces in the *Van der Waals*-equation of state $[m^5/(kgs^2)]$

A_{int} contact area between the gas in the tank and the tank wall $[m^2]$

b constant describing the finite volume of a molecule in the *Van der Waals*- and *Abel-Noble*-equation of state $[m^3/kg]$

c_v specific heat at constant volume $[J/(kgK)]$

$c_{p,fiber}$ Specific heat capacity of the fiber $[J/(kgK)]$

$c_{p,gas}$ Specific heat capacity of the gas at constant pressure $[J/(kgK)]$

$c_{p,liner}$ Specific heat capacity of the liner $[J/(kgK)]$

$c_{p,wall}$ specific heat capacity of the wall material $[J/(kgK)]$

D Diameter $[m]$

D_{inlet} Inlet diameter $[m]$

D_{int} Internal diameter of the tank $[m]$

f Friction factor $[-]$

g gravitational constant $[m/s^2]$

Gr Grashof number of the gas in the tank $[-]$

h_{int} Convective heat transfer coefficient between the gas in the tank and the tank wall $[W/(m^2K)]$

h_{in} specific inlet enthalpy $[J/kg]$

i index indicating which wall element is used

k_{ext} External convective heat transfer coefficient $[W/(m^2K)]$

L Length of the tank $[m]$

M_0 Momentum flux of the incoming hydrogen $[kgm/s^2]$

m_{ent} Entrainment mass of the hydrogen in the tank $[kg]$

m_{gas} Mass of the hydrogen in the tank $[kg]$

m_{inlet} Mass present in the inlet per time-step $[kg]$

n The amount of wall elements used in the simulation $[-]$

$Nu_{int,forced}$ Nusselt number corresponding to forced convection $[-]$

$Nu_{int,natural}$ Nusselt number corresponding to natural convection $[-]$

Nu_{int} Nusselt number of the gas $[-]$

P Pressure of the gas $[Pa]$

P_{ini} Initial pressure in the tank $[MPa]$

Pr Prandtl number of the gas $[-]$

PRR Pressure ramp rate $[MPa/s]$

Q Heat added/subtracted to/from the system $[J]$

R_{H_w} Hydrogen specific gas constant $[J/(kgK)]$

Re Reynolds number of the gas in the tank $[-]$

T Temperature $[K]$

t time of the simulation $[s]$

T_{amb} Ambient temperature $[K]$

T_{del} Gas delivery temperature $[K]$

$T_{gas,ini}$ Initial gas temperature $[K]$

T_{gas} Temperature of the gas in the tank $[K]$

$T_{wall,ini}$ Initial wall temperature $[K]$

$T_{wall,int}$ Internal temperature of the wall $[K]$

T_{wall} Wall temperature $[K]$

U internal energy of the gas $[J]$

u_{ent} Entrainment velocity of the hydrogen in the tank $[m/s]$

u_{gas} Velocity of the gas $[m/s]$

u_{inlet} Inlet velocity $[m/s]$

u_{tank} Characteristic velocity of the hydrogen in the tank $[m/s]$

V Volume of the tank $[m^3]$

v Specific volume of the gas $[m^3/kg]$

Greek symbols

α Thermal expansion coefficient of the gas $[1/K]$

Δx_f Element size of the fiber material $[m]$

Δx_L Element size of the liner material $[m]$

γ specific heats ratio $[-]$

μ_{gas} Dynamic viscosity of the gas $[Pas]$

ρ_{fiber} Density of the fiber material $[kg/m^3]$

ρ_{gas} Density of the gas $[kg/m^3]$

ρ_{inlet} Density of the hydrogen in the inlet $[kg/m^3]$

ρ_{liner} Density of the liner material $[kg/m^3]$

ρ_{wall} Density of the wall $[kg/m^3]$

k_{fiber} Conductivity of the fiber material $[W/(mK)]$

k_{gas} Conductivity of the gas $[W/(mK)]$

k_{liner} Conductivity of the liner material $[W/(mK)]$

k_{wall} Conductivity of the wall $[W/(mK)]$

1 Introduction

As the effects of climate change become more apparent, reducing greenhouse gas emissions becomes increasingly urgent. Inland shipping is one area where emissions can be significantly reduced. In the Netherlands, the inland waterways shipping industry is responsible for 13% of the total CO_2-emission and 37% of the total NO_x-emission of the total cargo transport sector [2]. To reduce these percentages, the Dutch government and representatives from the inland shipping sector have signed the *Green Deal on Maritime and Inland Shipping and Ports*. One of the targets in this deal is that by 2030, a total of 150 zero-emission cargo vessels will sail through the Dutch inland waterways [3].
Hydrogen (H_2) is a promising fuel for inland cargo shipping offering the potential to sail without any emission of greenhouse gasses (GHG) during the vessel's journey. The *H2-barge 1*, the world's first zero-emission inland cargo vessel, requires a total of 1000 kg of hydrogen fuel during a typical journey. This hydrogen is stored in two swappable containers, each consisting of 8 hydrogen tanks with a capacity of just over 60 kg at a pressure of 350 bar. The *H2-barge 1* is the pioneering vessel in *Future Proof Shipping*'s (FPS) initiative to expand its zero-emission fleet [1].
H_2 is used as a fuel in Proton Exchange Membrane (PEM) fuel cells where its molecules react with oxygen (O_2) in a redox reaction. During this reaction, electrons split from the ions and flow through a circuit to form an electrical current, see Figure 1.1.

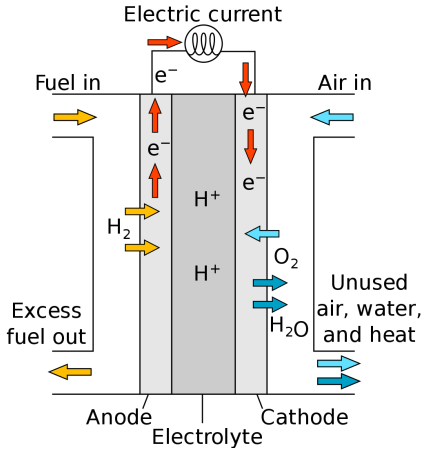

Figure 1.1: Schematic representation of the working principle of a PEM fuel cell [4]

The energy from this current will either be used in the onboard systems or stored in the battery systems present. Notably is that the sole waste product of this reaction is pure water.
A major issue that arises when using hydrogen as the fuel is the required space onboard the vessel. Per unit volume, hydrogen at 350 bar only contains one-tenth of the energy compared to diesel [5].
From the storage of hydrogen, the challenge extends to the corresponding refueling process, or bunkering as it is called in maritime applications. During a bunkering procedure of gaseous hydrogen, the temperature of the gas rises. The temperature limit for the gas is currently set at 85$^{\circ}C$ [6]. This limit is established to respect material limits of the components in the hydrogen supply system, to prevent over- and/or under-pressurization and to allow organizations to introduce consistency for different hydrogen vehicles and hydrogen refueling stations [6]. Safety measures, such as limiting the hydrogen inflow, manipulating the temperature of the incoming hydrogen, or managing the heat transfer away from the tank can be implemented to adhere to this limit.

Knowledge about refueling hydrogen in small-scale applications (tank sizes up to 150L) is more abundant as the automotive industry has already been using hydrogen as a fuel for over 10 years. In contrast to this, limited information is available for the refueling/bunkering for larger tank sizes [7]. When further increasing tank sizes beyond 150L, little knowledge on the behavior of hydrogen inside the tank is available [6].
Kesana [7] started addressing this knowledge gap. A CFD (computational fluid dynamics) simulation has been conducted to assess the behavior of the hydrogen inside a larger (1800L) fuel tank. A CFD simulation is an extensive tool that yields a detailed description of the behavior of hydrogen, including parameters such as flow vectors and magnitudes of the hydrogen elements inside the tank, heat transfer parameters and the temperature evolution of the hydrogen in the tank [8]. This amount of detail increased the complexity of the simulation, which ultimately took 24 days to finish using computer hardware specific to the job. A simulation this time-consuming cannot be used for quick assessments of hydrogen behavior inside a gas tank. This quick assessing of temperature response is a useful tool for companies such as FPS to support the decision-making process for a certain type of hydrogen storage solution. To address this limitation, this research will aim to construct a thermal simulation model in MATLAB/Simulink with a 0D gas model and a 1D wall model. This technique has already been applied in this field by Kesana [7], however, as the reproducible nature of this model is considered questionable, this research aims to enhance their model and identify the obstacles and potential improvements. The proposed model is expected to be finished within the minute, while still providing valuable insights for companies that (will) make use of a hydrogen cylinder for mobile applications.
The main research question corresponding to the aforementioned issue will be:

How to design a fast simulation tool for a hydrogen tank filling, from which the temperature evolution of both the gas and the tank wall can be observed?

To support the research question, the following sub-questions will be answered in this research as well:

1. *What are the theoretical principles behind a hydrogen tank filling?*
2. *How is the pressure of the delivered hydrogen controlled?*
3. *How does the model perform with respect to the research it is based on?*
4. *Are there potential improvements and/or points of interest in the existing model and how should they be addressed?*
5. *How do different input parameters impact the temperature development in the tank during hydrogen refueling?*

In chapter 2, the knowledge which is used in the model itself will be discussed and sub-questions 1 & 2 will be answered. In chapter 3, the construction of the model will be discussed and therefore sub-question 3 will be answered. chapter 4 will guide the reader through the validation process in which the performance of the model will be discussed (sub-question 4) and it will also cover some improvements that are performed in the model, therefore also answering sub-question 5. chapter 5 will discuss the results of a parameter study. chapter 6 will discuss the performance of the simulation model that is used in this research and will also contain recommendations for future work. To conclude this thesis, chapter 7 will answer the research question and all corresponding sub-questions.

2

Literature review

This section will be dedicated to explaining the theoretical principles that are used to describe the filling procedure of a hydrogen tank. Apart from the theoretical part is useful to gain insight into the equipment that is used to maintain a certain pressure ramp rate (PRR), which is an important parameter in the construction of the simulation model. In this chapter, the following sub-questions will be answered:

- *"What are the theoretical principles behind a hydrogen tank filling?"*
- *"How is the pressure of the delivered hydrogen controlled?"*

2.1. Thermodynamic behaviour of hydrogen

In this section, the thermodynamic behaviour of hydrogen that occurs during refuelling will be covered. The thermodynamic behaviour can be computed with an equation of state and the first law of thermodynamics, which will respectively be introduced in subsection 2.1.1 and subsection 2.1.2. Subsection 2.1.3 will introduce the *entrainment* velocity of hydrogen. This is an important parameter for determining the *Reynold's* number, which will be covered in subsection 2.2.1.

2.1.1. Abel-Noble equation of state

The equation of state is an expression in which the physical conditions of the gas (temperature, pressure, volume and internal energy) are related. A simplified but useful approach to describe the thermodynamic behaviour is the *ideal gas model*, see Equation 2.1 [9].

$$Pv = R_{H_2}T \tag{2.1}$$

Where P is the pressure of the gas, v is the specific volume of the gas, R_{H_2} is the specific gas constant and T is the temperature of the gas. In this model, the interaction between separate gas molecules is left out. This model is valid in many engineering applications, however when taking larger pressures (>100 bar) into account, a non-linear relation between the pressure and the density of a gas becomes apparent. This is due to an increased interaction due to a tighter packing of the molecules, therefore

increasing the total number of interactions. This interaction is taken into account in the *Van der Waals*-equation, which is a further development of the ideal gas model, see Equation 2.2:

$$\left(P + \frac{a}{v^2}\right)(v - b) = R_{H_2}T \tag{2.2}$$

Where P is the pressure in the system, a is the factor in Equation 2.2 which accounts for the inter-molecular attraction forces, v is the specific volume of the gas, b is the factor which takes the finite volume of molecules into account, R_{H_2} is the universal gas constant and T is the temperature of the gas. In the *Van der Waals*-equation, factor a represents the inter-molecular interaction. When considering gas systems consisting of either hydrogen, helium or neon, the molecules are so light that the inter-molecular interaction can be neglected. Considering this, the *Van der Waals*-equation is simplified to an equation with only a single gas-specific parameter (b) [10]:

$$P(v - b) = R_{H_2}T \tag{2.3}$$

In Equation 2.3, it should be noted that the value of b deviates from the hydrogen specific value that is valid when using the *Van der Waals*-equation, as is derived by Michler [11].

By isolating T from Equation 2.3 and using the relation $v = \frac{1}{\rho}$, the following expression for the gas temperature can be established:

$$T = \frac{P(1 - b\rho)}{\rho R_{H_2}} \tag{2.4}$$

where ρ is the density of the gas.

2.1.2. First law of thermodynamics

The first law of thermodynamics is the energy balance of a system, in this research, the system will be a hydrogen tank. It states that the change in energy in the system is the sum of the heat transfer and the work done on the system, which is described in Equation 2.5:

$$\frac{dU}{dt} = \frac{dQ}{dt} + h_{in}\dot{m}_{gas} \tag{2.5}$$

Where $\frac{dU}{dt}$ is the rate of change of the energy in the system, $\frac{dQ}{dt}$ is the heat added to the system, h_{in} is the enthalpy of the incoming gas and $\dot{m}_{gas}$ is the mass flow rate of the gas.

2.1.3. Entrainment of a gas

Hydrogen enters a tank through a nozzle as a jet stream. This jet stream entrains stationary hydrogen which has already been inside the tank along with the hydrogen that just entered the tank. As the jet stream happens in a hydrogen tank, the jet is enclosed and can therefore be considered as a confined jet. This process is called entrainment and is visualized in Figure 2.1.

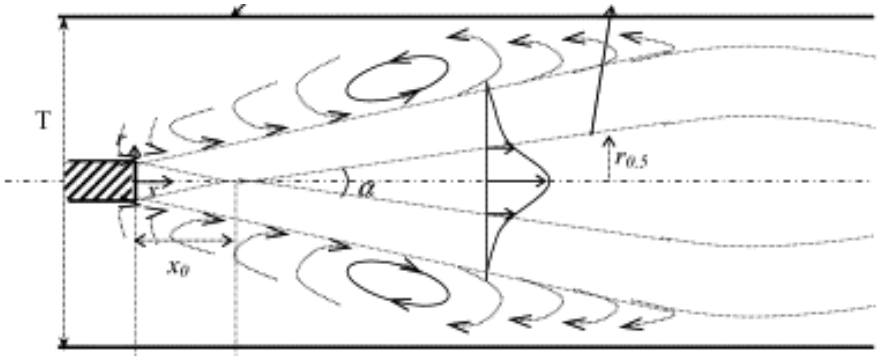

Figure 2.1: Schematic representation of entrainment of a gas by a confined jet [12]

During the entrainment of gas, additional mass is entrained by the jet into the stream, meaning that the mass flow rate of the jet increases with the distance from the nozzle until the jet dissipates in the tank. The location of the dissipation of the jet depends on the inlet diameter and the dimensions of the tank [13].
The importance of entrainment in this part lies in the calculation of a characteristic velocity of hydrogen, which is used to calculate the *Reynolds* number (see subsection 2.2.1). The kinetic energy due to the characteristic velocity is the sum of the kinetic energy of the inlet velocity and the entrainment velocity:

$$\frac{m_{gas}(u_{tank})^2}{2} = \frac{m_{ent}(u_{ent})^2}{2} + \frac{m_{inlet}(u_{inlet})^2}{2} \tag{2.6}$$

where m_{gas} is the mass of the gas in the tank, u_{tank} is the characteristic velocity of the gas in the tank, m_{ent} is the entrainment mass, u_{ent} is the entrainment velocity, m_{inlet} is the inlet mass which is calculated by taking the product of the inlet mass flow rate and the time-step of the simulation, and u_{inlet} is the inlet velocity of the gas. In this expression for the kinetic energy of the gas, the entrainment mass of the gas is assumed to be equal to the mass of the gas in the tank. For smaller tanks, this assumption can be considered as valid as all gas in the tank participates in the turbulent behavior. However, when increasing the size of the tank, a portion of the gas in the tank will become stagnant, which will induce a difference between m_{tank} and m_{ent}. The entrainment velocity can be calculated by determining the inlet velocity u_{inlet} (Equation 2.7), the momentum flux of the incoming hydrogen M_0 (Equation 2.8) and the entrainment mass flow rate $\dot{m}_{ent}$ (Equation 2.9) [14].

When the mass flow rate is known, the velocity of a fluid flowing through a body with a circular cross-section can be calculated as follows:

$$u_{inlet} = \frac{4\dot{m}_{gas}}{\rho_{gas}(D_{inlet})^2\pi} \tag{2.7}$$

$$M_0 = \frac{1}{4}\pi(D_{inlet})^2\rho_{inlet}(u_{inlet})^2 \tag{2.8}$$

$$\dot{m}_{ent} = 0.282(M_0)^{0.5}(\rho_{gas})^{0.5}L \tag{2.9}$$

$$u_{ent} = \frac{4\dot{m}_{ent}}{\rho_{gas}(D_{int})^2\pi} \tag{2.10}$$

2.2. Convective heat transfer

The heat transfer between a fluid and a solid, in this case the tank wall, is called convective heat transfer. It can be calculated according to Equation 2.11:

$$\frac{dQ}{dt} = h_{int} A_{int} (T_{wall,int} - T_{gas}) \tag{2.11}$$

where $\frac{dQ}{dt}$ is the heat transfer between gas and tank, h_{int} is the internal convective heat transfer coefficient, A_{int} is the contact area between gas and solid, $T_{wall,int}$ is the internal temperature of the tank wall in contact with the gas and T_{gas} is the gas temperature.
k_{int} is calculated according to Equation 2.12:

$$h_{int} = \frac{k_{gas} Nu_{int}}{D_{int}} \tag{2.12}$$

Where k_{gas} is the conductivity of the gas and Nu_{int} is the *Nusselt*-number of the gas. The *Nusselt*-number depends on the convection regime which is present, this can be forced (subsection 2.2.1), natural (subsection 2.2.2) or a combination of both. Forced convection occurs in a system where the gas is in strong motion, whereas natural convection occurs when the gas is stationary and mainly dependent on buoyancy- and viscous effects. The ratio between the *Grashof*-number and the square of the *Reynolds*-number ($\frac{Gr}{Re^2}$) is a measure to determine which convection regime (forced, natural, or a combination) occurs [15]:

$$\begin{cases} \text{if } \frac{Gr_{tank}}{(Re_{tank})^2} < 0.1,\ h_{int} = h_{int,forced} \\ \text{if } 0.1 < \frac{Gr_{tank}}{(Re_{tank})^2} < 10,\ h_{int} = (k_{int,natural}^4 + h_{int,forced}^4)^{\frac{1}{4}} \\ \text{if } \frac{Gr_{tank}}{(Re_{tank})^2} > 10,\ h_{int} = h_{int,natural} \end{cases} \tag{2.13}$$

where the Gr_{tank} is the *Grashof*-number in the tank and Re_{tank} is the *Reynolds*-number in the tank. The *Grashof*-number is a ratio between buoyancy effects and viscous effects in the gas. The Grashof number in a tank is calculated as follows [15]:

$$Gr_{tank} = \frac{g\alpha |T_{gas} - T_{wall,int}| \rho_{gas}^2 D_{int}^3}{\mu_{gas}^2} \tag{2.14}$$

where g is the gravitational constant, ρ_{gas} is the density of the gas, D_{int} is the internal diameter of the tank and μ_{gas} is the dynamic viscosity of the gas.
The *Reynolds*-number is a ratio between inertial effects and viscous effects in the gas, with an increasing Reynolds number, the turbulent motion of the gas also becomes more apparent. The characteristic Reynolds number in the tank is calculated as follows:

$$Re_{tank} = \frac{\rho_{gas} u_{tank} D_{int}}{\mu_{gas}} \tag{2.15}$$

where u_{tank} is the characteristic velocity of the hydrogen in the tank, as is explained in subsection 2.1.3.

Depending on the convection regime, the *Nusselt*-number is calculated differently. The calculation of the *Nusselt*-number will be covered in subsection 2.2.1 and subsection 2.2.2.

2.2.1. Forced convection

Forced convection occurs when the gas is in turbulent motion. The *Nusselt*-number is computed according to empirical relations, which have been developed in several pieces of research. The *Gnielinski*-equation is considered as a suitable approach to compute the *Nusselt*-number in forced convection regimes [15, 16]:

$$Nu_{int,forced} = \frac{(f/8)(Re_{tank} - 1000)Pr}{1 + 12.7(f/8)^{0.5}(Pr^{2/3} - 1)} \tag{2.16}$$

Equation 2.16 is valid under the following conditions:

$$\begin{cases} 0.5 \leq Pr \leq 2000 \\ 3 * 10^3 < Re < 5 * 10^6 \end{cases} \tag{2.17}$$

Where f is the friction factor, Re_{tank} is the *Reynolds* number in the tank and Pr is the *Prandtl*-number of the gas. The friction factor of the gas is a dimensionless parameter related to the shear stress in the gas. Due to the smooth nature of the wall inside the tank, the following expression for the friction factor will be used:

$$f = \frac{1}{(0.790ln(Re_{tank}) - 1.64)^2} \tag{2.18}$$

The $Prandtl$-number is a dimensionless parameter that describes the thickness of the thermal boundary layer, which is a layer that appears when a fluid flows over a solid which is at a different temperature, its expression is [15]:

$$Pr = \frac{\mu_{gas} c_{p,gas}}{k_{gas}} \tag{2.19}$$

2.2.2. Natural convection

Natural convection is, in contrast to forced convection, a passive type of convection, where the *Nusselt*-number is based on buoyancy effects that occur due to local temperature (and therefore density) variations in the gas. An equation of the *Nusselt*-number in hydrogen applications has been established [15, 17]:

$$Nu_{int,natural} = 0.104 \left(\frac{g\alpha |T_{gas} - T_{wall,int}| c_{p,gas} (\rho_{gas})^2 D_{int}^3}{\mu_{gas} k_{gas}} \right)^{0.352} \tag{2.20}$$

A common parameter used to quantify natural convection is the *Rayleigh*-number, which is the product of the *Grashof*- and the *Prandtl* number. The term that stands between brackets in Equation 2.20 is the Rayleigh number.

2.3. Conductive heat transfer

To provide a detailed temperature evolution of gas inside a cylinder during a bunker procedure, it is important to know the wall temperature. The wall temperature itself evolves due to the increase of gas temperature within the cylinder, but what factors contribute to the change in the wall temperature? Important parameters are the material-specific properties of the wall, which will be discussed in subsection 2.3.1.

2.3.1. Wall properties

The wall of a typical hydrogen tank is composed of 2 separate layers: a liner element and a fiber element. Due to weight considerations, tank types III and IV are relevant for mobile purposes, among which are inland shipping solutions. These tank types have a liner of either aluminum (type III) or a lighter polymer (type IV). The liner element of the wall is a thin layer that seals the hydrogen inside the tank. The liner is wrapped with carbon- or glass fibers, which account for the structural strength of the hydrogen tank [18, 19].

The relevant properties to describe the thermal behavior of the wall materials are the density ρ, specific heat capacity c_p and conductivity k of the material.

The governing equation that describes the heat transfer through the tank wall is as follows:

$$\rho_{wall} c_{p,wall} \frac{dT_{wall}}{dt} = \frac{d}{dx}\left(k_{wall} \frac{dT_{wall}}{dx}\right) \tag{2.21}$$

Where ρ_{wall} is the density of wall material, $c_{p,wall}$ the specific heat capacity of the wall material, $\frac{dT_{wall}}{dt}$ the temperature evolution of the wall over time, k_{wall} the conductivity of the wall material and $\frac{dT_{wall}}{dx}$ the temperature evolution of the wall over the width of the wall. The specific heat capacity of the wall states how much energy is needed for a temperature rise of 1K per kg material, whereas the conductivity of the wall states how much energy can be transferred through the wall. The thermal inertia of the wall is a function of the conductivity, specific heat capacity and density of the wall material.

2.4. Conclusion

In this chapter, the theory behind a tank filling has been investigated. Two substantial components are related to the gas: the thermodynamic behavior and the gas dynamics. The thermodynamic behavior of the gas is the component in which the heat generation due to the gas supply is described and in the gas-dynamics part the heat transfer coefficients of the gas to the tank are determined.

3

Methodology

The theoretical principles of the required simulation model have been explained in chapter 2, this chapter will explain the translation of these principles into a working simulation model, which is based on the model used by Kesana [7]. The software which will be used to set up the simulation will be MATLAB/Simulink. MATLAB will serve in this part as a useful tool for pre- and post-processing of the data, whereas simulink will be the core of the simulation due to its intuitive nature and experience of the author with the software.

3.1. Simulation model

The simulation will be conducted using a quasi-static model. The quasi-static approach can be considered valid when simulating the filling of a hydrogen tank because there is only a slight change in equilibrium between two consecutive states. This change is induced by two factors: the extra hydrogen added to the system, and the heat exchange between the gas and the wall of the tank [9]. The quasi-static nature of the simulation allows to extraction of the following steady-state parameters from look-up tables which have been experimentally established by the NIST [20]:

- Specific heat capacity, $c_{p,gas}$
- Dynamic viscosity, μ_{gas}
- Gas conductivity, k_{gas}

The input parameters of the model can be found in Table 1. The external heat transfer coefficient is set at a constant rate. Its value is a representative value for an object in still air [21]. chapter 4 will zoom in on the validity of this value.
The parameters listed in Table 1 will be used to solve the simulation, by computing a loop of calculations for every time step, see Figure 3.1.

Parameter	Base model value
Pressure Ramp Rate (PRR)	$0.0275\ MPa/s$
gravitational constant (g)	$9.81\ m/s^2$
Initial gas pressure in tank (P_{ini})	$2\ MPa$
Tank volume (V)	$1.8\ m^3$
Tank diameter (D_{int})	$0.65\ m$
Tank length (L_{tank})	$5.42\ m$
Nozzle diameter (D_{inlet})	$0.004\ m$
Initial wall temperature ($T_{wall,ini}$)	$293\ K$
Initial gas temperature ($T_{gas,ini}$)	$293\ K$
Ambient temperature (T_{amb})	$300\ K$
Gas delivery temperature (T_{del})	$293\ K$
Liner density (ρ_{liner})	$945\ kg/m^3$
Liner specific heat capacity ($c_{p,liner}$)	$1580\ J/(kgK)$
Liner conductivity (k_{liner})	$0.48\ W/(mK)$
Liner element size (Δx_L)	$0.001\ m$
Fiber density (ρ_{fiber})	$2051\ kg/m^3$
Fiber heat capacity ($c_{p,fiber}$)	$878\ J/(kgK)$
Fiber conductivity (k_{fiber})	$0.113\ W/(mK)$
Fiber element size (Δx_c)	$0.001\ m$
External heat transfer coefficient (h_{ext})	$6\ W/(m^2K)$

Table 1: Input parameters of the simulation model

The external heat transfer coefficient is set at a constant rate. Its value is a representative value for an object in still air [21]. chapter 4 will zoom in on the validity of this value.
The parameters listed in Table 1 will be used to solve the simulation, by computing a loop of calculations for every time step, see Figure 3.1.

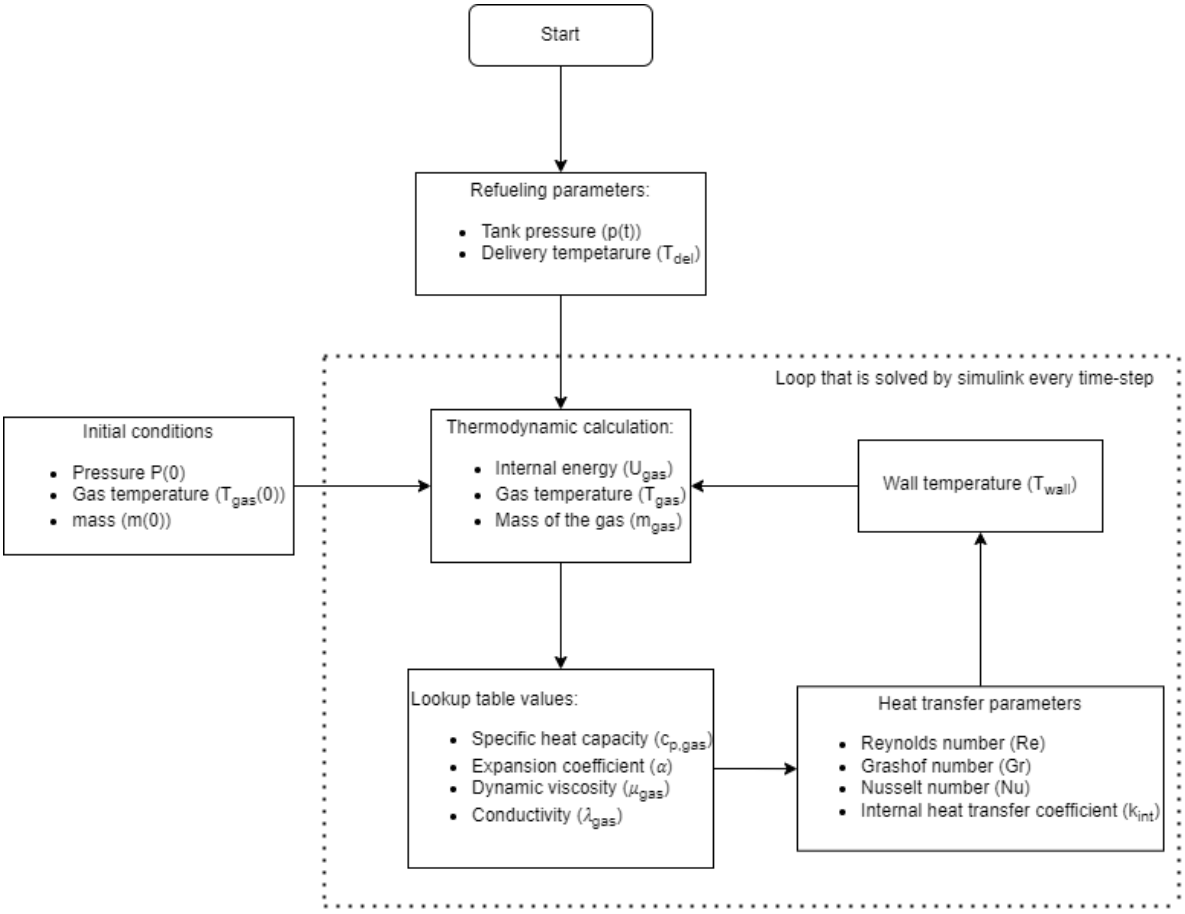

Figure 3.1: Schematic overview of the calculation process for every time-step

3.2. Governing equations

The parameters that are listed in section 3.1 will be used in the calculation process, as visualized in Table 1. These parameters will be used in the equations that have been introduced in chapter 2. The core of the simulation will consist of the *Abel-Noble*-equation of state (Equation 2.3), the equation of convective heat transfer (Equation 2.12) and the equation of wall temperature (Equation 2.21). These equations, and the equations which are derived from those, will together serve to determine the temperature of both the gas and the wall. The computation of both the mass flow rate and the wall temperature requires an introduction, which will be given in respectively subsection 3.2.1 and subsection 3.2.2.

3.2.1. Mass flow rate

The mass flow rate, ($\frac{dm_{gas}}{dt}$), is one the leading parameters in this model, it is calculated by combining the equation of the gas temperature according to the *Abel-Noble*-equation of state and the 1^{st} law of thermodynamics into the following equation [14]:

$$\frac{dm_{gas}}{dt} = \frac{\frac{dP_{gas}}{dt}\frac{(V-m_{gas}*b)}{\gamma-1} - h_{int} * A_{int}(T_{wall,int} - T_{gas})}{\frac{P_{gas}}{\gamma-1} * b + c_{p,gas}T_{del}} \tag{3.1}$$

3.2.2. Wall temperature

Due to material-specific properties, the heat will flow at different rates through the wall at different regimes:

1. Convection on the inside of the tank
2. Conduction through the liner
3. Conduction through the fiber
4. Convection on the outside of the tank

For all different regimes, the heat flux experiences a resistance against temperature change due to specific conditions per regime. The different resistances can be visualized using a resistance scheme that originates from the electrical analogy, see Figure 3.2.

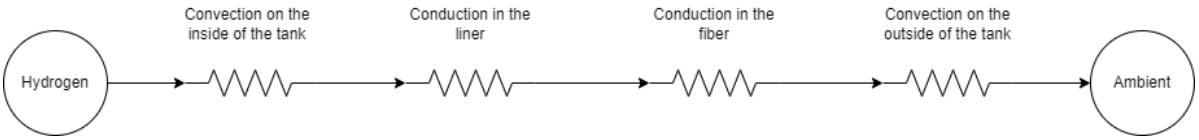

Figure 3.2: Schematic overview of the different resistances of the wall

Equation 2.21 is the mathematical expression for the wall temperature. Its implementation in the simulation model is proposed by Klopcic [22] and will be discussed in this part.
The wall will be divided into a finite amount of elements, each having a uniform temperature. For every element, an energy balance is established, where the heat flux is based on the temperature difference between the adjacent elements. Here-after the temperature will be computed by dividing the internal energy by the product of density, specific heat capacity and volume. In the wall temperature model, there are three locations of interest:

- The inner element where convective heat transfer takes place, from respectively the hydrogen in the tank to the inner element
- The transition between different wall materials, from liner to the fiber wrapping
- The outer element, where heat exchange between tank and environment takes place

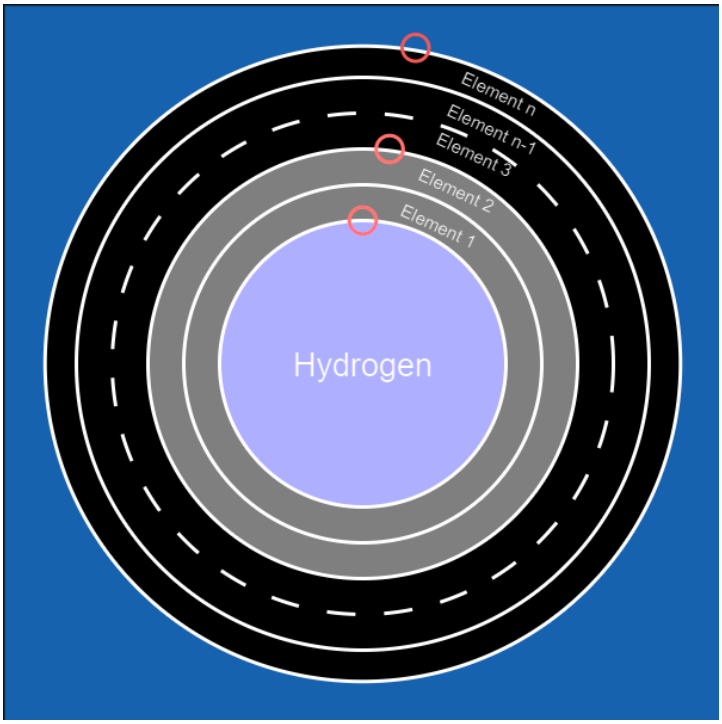

Figure 3.3: Schematic representation of the wall with hydrogen marked as the purple part, the liner marked as the grey part, the fiber area marked as the black part and the ambient region marked in blue. The dotted line indicates a jump to the 2 outer elements in the wall. The locations of interest as discussed above are marked with a red circle

For the inner and the outer elements where convective heat transfer takes place the energy balance is fairly straightforward. Equation 3.2 shows the expression for the temperature evolution in the first wall element:

$$\frac{\Delta T_{wall,1}}{\Delta t} = \frac{A_1 k_{int}(T_{gas} - T_{wall,1}) - A_2 \frac{k_{liner}}{\Delta x_{liner}}(T_{wall,1} - T_{wall,2})}{\rho_{liner} c_{p,liner} V_1} \tag{3.2}$$

Where $T_{wall,1}$ is the temperature of the first wall element, A_1 is the contact area between the gas and the first wall element, k_{int} is the convective heat transfer coefficient between the gas and the wall, T_{gas} is the temperature of the gas in the tank, A_2 is the contact area between the first and second wall element, k_{liner} is the conductivity of the liner, Δx_{liner} is the element size of the liner element, $T_{wall,2}$ is the temperature of the second wall element, ρ_{liner} is the density of the liner, $c_{p,liner}$ is the specific heat capacity of the liner and V_1 is the volume of the first wall element.
Equation 3.3 shows the expression for the temperature evolution in the final wall element:

$$\frac{\Delta T_{wall,n}}{\Delta t} = \frac{A_n \frac{k_{fiber}}{\Delta x_{fiber}}(T_{wall,n-1} - T_{wall,n}) - A_{n+1} k_{ext}(T_{wall,n} - T_{amb})}{\rho_{fiber} c_{p,fiber} V_n} \tag{3.3}$$

Where $T_{wall,n}$ is the temperature of the last wall element, $A_n - 1$ is the contact area between the second last wall element and the last wall element, k_c is the conductivity of the fiber, Δx_c is the element size of the fiber element, $T_{wall,n-1}$ is the temperature of

the second last wall element, k_{ext} is the convective heat transfer coefficient between the wall and the surrounding air, T_{amb} is the temperature of the surrounding air, A_{n+1} is the contact area between the last wall element and the surrounding air, ρ_c is the density of the liner, $c_{p,c}$ is the specific heat capacity of the liner and V_n is the volume of the last wall element.

However, some attention should be paid to the modeling of the heat transfer at the location where the liner ends and the fiber wrapping begins. The transition is modeled in the equation as $\frac{k_L+k_c}{\Delta x_L+\Delta x_C}$, to establish a balance between the conductance of the different materials see also Equation 3.4. It should be emphasized that Equation 3.4 is an equation that is still subject to improvement which will be discussed in chapter 4, it is **not** the definitive equation for a transition between materials.

$$\frac{\Delta T_{wall,i}}{\Delta t} = \frac{A_i \frac{k_{liner}}{\Delta x_{liner}}(T_{wall,i-1} - T_{wall,i}) - A_{i+1}\frac{k_{liner}+k_{fiber}}{\Delta x_{liner}+\Delta x_{fiber}}(T_{wall,i} - T_{wall,i+1})}{\rho_{liner} c_{p,liner} V_i}$$

$$\frac{\Delta T_{wall,i+1}}{\Delta t} = \frac{A_{i+1}\frac{k_{liner}+k_{fiber}}{\Delta x_{liner}+\Delta x_{fiber}}(T_{wall,i+1} - T_{wall,i}) - A_{i+2}\frac{k_{fiber}}{\Delta x_{fiber}}(T_{wall,i+1} - T_{wall,i+2})}{\rho_{fiber} c_{p,fiber} V_{i+1}} \tag{3.4}$$

where $\frac{\Delta T_{wall}}{\Delta t}$ indicates the change of the wall temperature over time, subscript i indicates the last liner element, subscript $i+1$ indicates the first fiber element, A is the area of the wall element, k is the conductivity of the material, subscript L indicates that the corresponding value belongs to the fiber part, subscript c indicates that the corresponding value belongs to the carbon fiber part, T_{wall} is the wall temperature, ρ is the density of the wall element, c_p is the specific heat capacity of the wall element and V is the volume of the wall element.

3.3. Conclusion

This chapter was dedicated to describing the equations which are used in the simulation. A substantial part of these equations were already discussed in chapter 2 and are straightforward to implement, however, the equations discussed in this chapter were not directly straightforward. The mass flow rate is determined based on the equations discussed in chapter 2 and the strategy of modeling the thermal response of the wall is also discussed. Its underlying formula was already known, but in the transition between gas and wall (and vice versa) and between the liner region and the fiber region demanded extra explanation which is provided in this chapter. The components discussed in this chapter allow to build the simulation model as required.

4

Validation

The first part of this chapter, section 4.1 will discuss and validate the output of the model, whose build-up has been explained in chapter 3. In this section, the mass flow rate and the compressibility of the gas as computed by the *Abel-Noble* equations of state will be compared to With the model set up, a few interesting points in the wall model have been observed. First of all in Equation 3.4 the transition between the liner is modeled in a non-robust manner while using the term $\frac{k_{liner}+k_{fiber}}{\Delta x_{liner}+\Delta x_{fiber}}$. This will be closely examined in this chapter in section 4.2.
Another point of interest is the resolution of the wall model. More wall elements mean that a more accurate representation of the wall temperature can be generated, but it will also result in a higher computational time, as there are more elements of which the temperature will be computed. The increase in resolution of the model will be assessed in section 4.3. Finally, the external heat transfer coefficient will be tested. As a constant value is assumed for the external heat transfer coefficient, the response to different heat transfer coefficient values should be tested before accepting this assumption. By investigating the previously mentioned aspects, the following research questions will be answered.

- *How does the model perform with respect to the research it is based on?*
- *Are there potential improvements in the existing model? If yes, how should they be addressed?*

4.1. Validating the model

In this section, the agreement between the output of the model of Kesana [7] and the model that has been set up during this research will be checked. As temperature is the parameter of interest in this research, the temperature evolution will be compared to the model constructed by Kesana. Next to the temperature evolution, both the mass flow rate and the compressibility of the gas will be compared to computed output and output that is extracted from look-up tables consisting of experimentally constituted data by the *National Institute of Standards and Technology* (NIST)[20].

4.1.1. Mass flow rate

In the simulation model, the mass flow rate is calculated according to Equation 3.1. To validate this approach, the mass flow rate has also been computed by extracting the density as a function of temperature and pressure ($\rho(p,T)$) at every time-step of the simulation and taking its derivative ($\dot{\rho}$). When multiplying $\dot{\rho}$ with the volume of the tank, the following relation is established:

$$\dot{m} = \dot{\rho} * V \tag{4.1}$$

Both expressions for the mass flow rate have been visualized in Figure 4.1. There is only a slight difference, no more than 2% in the plots, which indicates a valid computation for the mass flow rate. The drop in Figure 4.1 at 1200 s occurs at the instance where the hydrogen supply stops and therefore $\dot{m}$ will be zero from this point. The change in density however will still be non-zero due to the cooling of the gas. Equation 4.1 is valid during the supply of hydrogen, after the target pressure is reached, the simulation model will set $\dot{m}$ to zero.

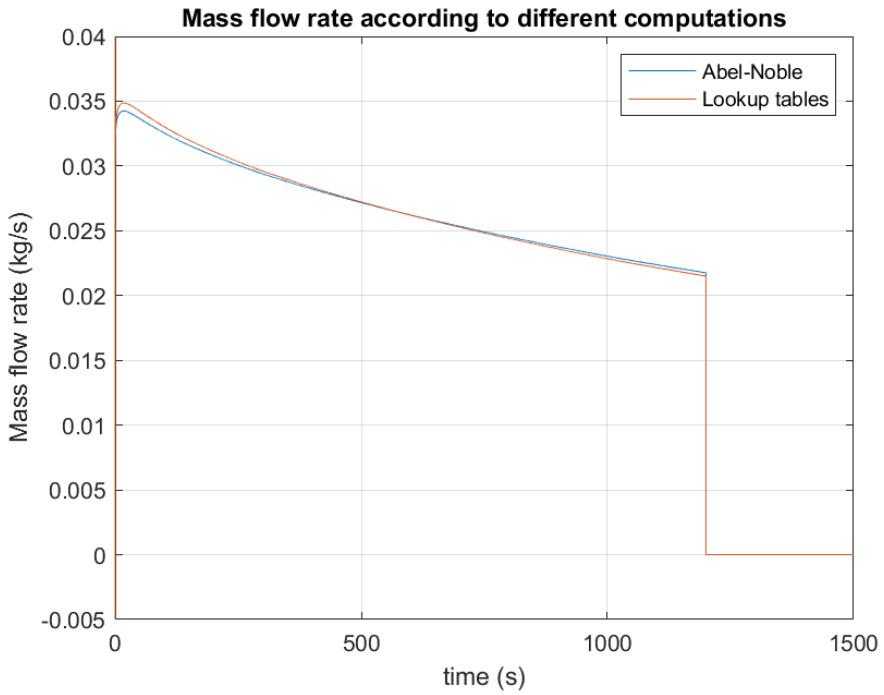

Figure 4.1: Computation of $\dot{m}$ according to both the *Abel-Noble* gas model and look-up tables

4.1.2. Compressibility

Figure 4.2 shows the compressibility of the gas according to experimental data obtained by the NIST [20] and the compressibility computed according to the *Abel-Noble* gas model. The compressibility is in agreement with the mass flow rate since a lower compressibility of gas means that per extra unit of pressure, the density changes at a higher rate and therefore a higher compressibility corresponds with a lower mass flow rate.

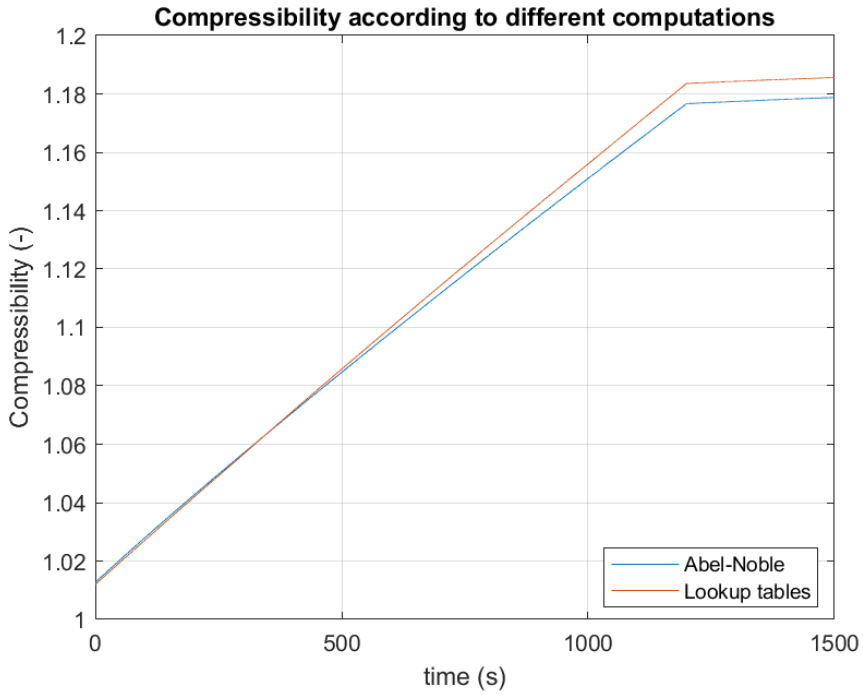

Figure 4.2: Computation the compressibility according to both the *Abel-Noble* gas model and look-up tables

4.1.3. Temperature evolution

The focus point of this research is the temperature evolution of the hydrogen in the tank. To assess the performance of this model, it has been compared to both a very large hydrogen tank with a volume of 1800L and a small hydrogen tank with a volume of 29L. The corresponding data originates from respectively Kesana [7] and De Miguel [23]. A first observation that can be made is that for the different tank volumes, different temperature offsets with respect to the research data can be observed. For the small tank, a positive offset of $+20°C$ can be observed, whereas for the large tank, the offset becomes $+5°C$. This raises a question on whether the model used by Kesana [7] and Molkov [14] is fully reproducible based on the information that has been provided, given the positive offset in both cases and the difference in offset. This difference in offset between the large and small tanks marks a major shortcoming of a lumped gas model. The large hydrogen tank is according to the simulation model considered to be in a forced convection regime for the complete filling, however, Kesana found in the CFD simulation that only in the first 28% of the tank, as seen from the nozzle, hydrogen mixing takes place [7]. This indicates that in the first part of the tank forced convection is likely to take place, however in the part after this it is likely that natural convection is the leading convection regime. The consequence of this statement is that the convectional heat transfer coefficient is likely to be over-estimated.

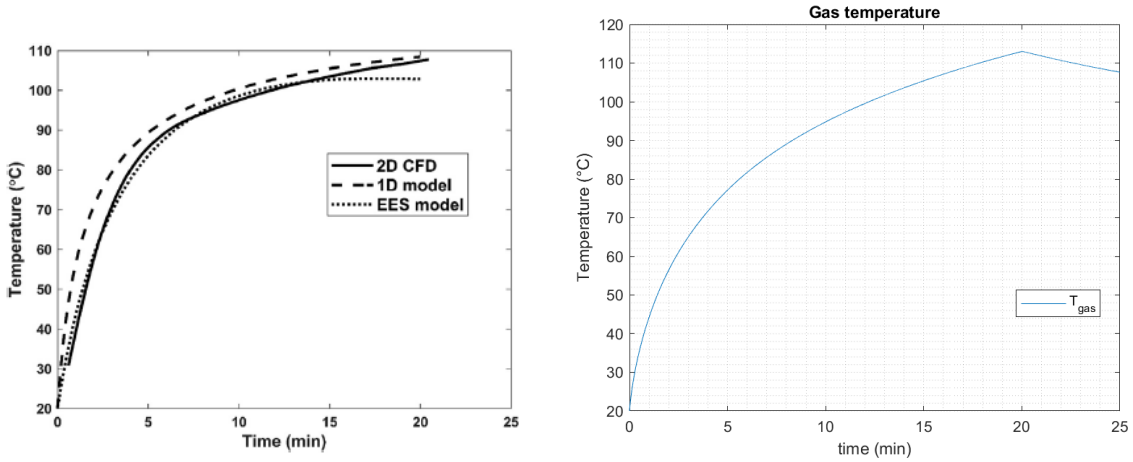

(a) Temperature evolution computed by Kesana [7]

(b) Temperature evolution as computed by the own model

Figure 4.3: Comparison of the temperature evolution of model by Kesana and the model constructed in this research

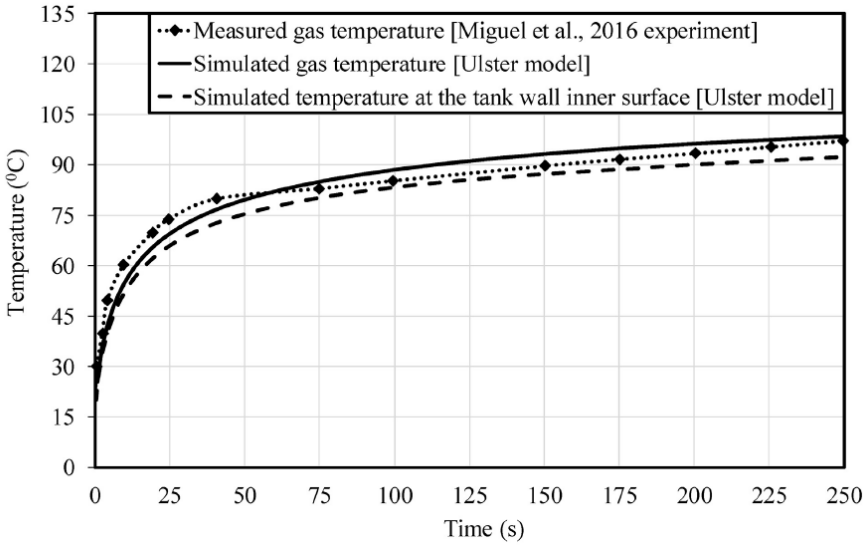

(a) Temperature evolution of a 29L hydrogen tank filling obtained by De Miguel [23]

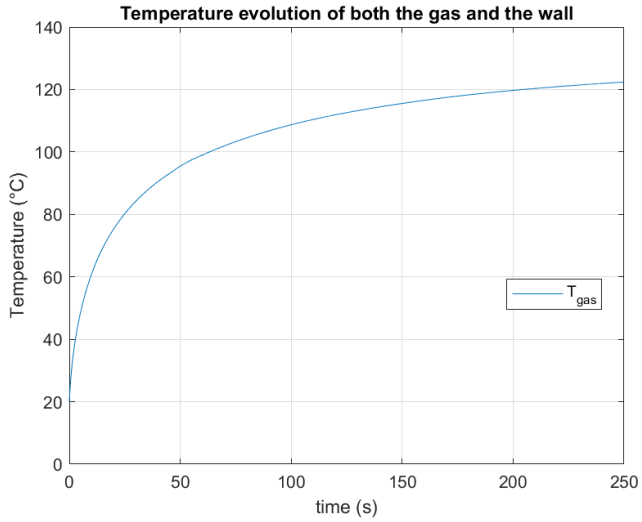

(b) Temperature evolution of a 29L hydrogen tank filling, obtained from own model

Figure 4.4: Comparison of the temperature evolution of model by De Miguel and the model constructed in this research

4.2. Transition between materials

The conductance of the interface between the two wall materials is currently modeled as $\frac{k_{liner}+k_{fiber}}{\Delta x_{liner}+\Delta x_{fiber}}$. This expression equals the average value of both separate conductances, computed as $\frac{1}{2}\left(\frac{k_{liner}}{\Delta x_{liner}}+\frac{k_{fiber}}{\Delta x_{fiber}}\right)$, taking into account that $\Delta x_{liner} = \Delta x_{fiber}$. However, the original expression implies that Δx_{liner} and Δx_{fiber} may have different values. However, in the current form, the expression for conductance at the transition cannot be a function of the conductance for the adjacent wall elements when $\Delta x_{liner} \neq \Delta x_{fiber}$. To make the equation suitable for applications where different element sizes are used, the following expression is recommended:

$$Co_{transition} = \frac{k_{liner}\Delta x_{fiber} + k_{fiber}\Delta x_{liner}}{2\Delta x_{liner}\Delta x_{fiber}} \tag{4.2}$$

Where $Co_{transition}$ is the conductance at the transition between materials.

4.3. Resolution of the wall

In section 4.1, the resolution of the liner part of the wall is set at 1 mm and that of the fiber part is set at 3 mm. The setting of the resolution is a trade-off between accuracy and computational effort, namely a higher resolution means a higher amount of calculations to be performed. However, it is important to investigate the effects of the resolution of the wall and what would be the best option for running the simulation itself. To solve the problem mentioned above, 3 different resolutions will be compared to each other: a resolution with an element size of 0.5 mm, a resolution with an element size of 1 mm and one with an element size of 3 mm. A special case already occurs when determining the gas- and wall temperature for an element size of 3 mm, since this indicates that the liner part of the wall will only consist of 1 element. It is interesting to see how this will affect the temperature curve.
Figure 4.5 and Figure 4.6 show respectively the wall temperature at the end of the filling of the tank and the evolution of the gas temperature over time. The first thing to notice from Figure 4.5 is that a resolution of 3mm for the liner part does not provide a realistic depiction. The temperature declines at a high rate with respect to an increasing wall thickness right from the beginning of the wall, whereas with both a resolution of 0.5 mm and 1 mm, the thermal effect of a transition between different materials can be observed rather well. All simulations are finished nearly instantaneous ($< 20s$) and the difference in maximum temperature between simulations with different wall resolutions is negligible.

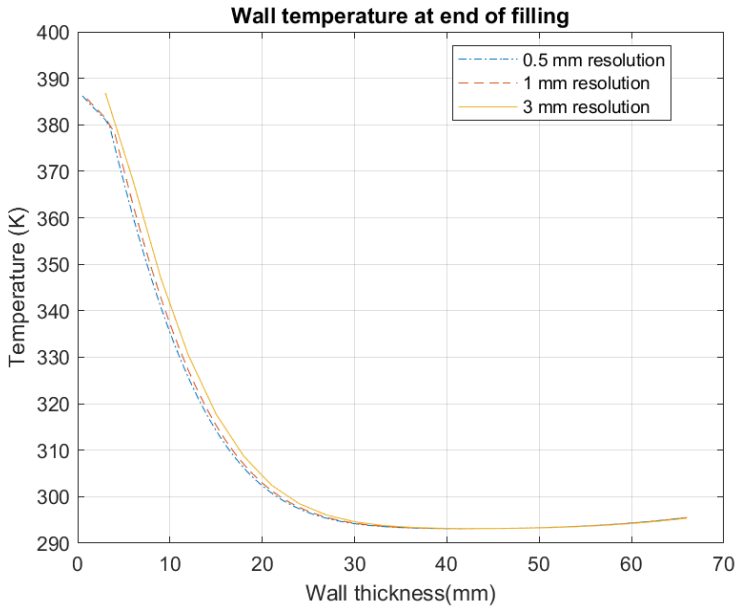

Figure 4.5: Wall temperature at the end of filling, for different resolutions

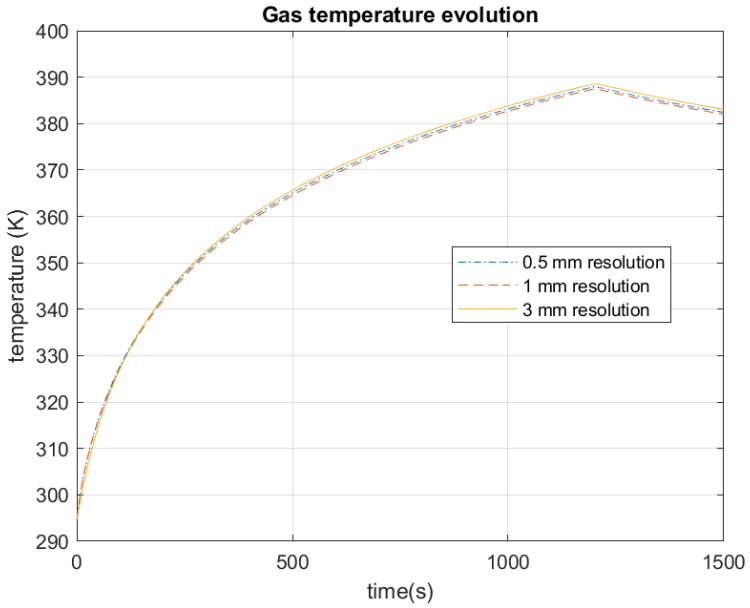

Figure 4.6: Gas temperature evolution at different resolutions

4.4. External heat transfer coefficient

Currently, the external heat transfer coefficient is set at a constant value of $6W/(m^2K)$. It follows that for an object in still air, values for h_{ext} are in the range of $2.5-25W/(m^2K)$. For an object in air that is subject to forced convection, the values range between $10-500W/(m^2K)$. To validate the assumption that a constant value for the external heat transfer coefficient is sufficient in this research, three different values for the external heat transfer coefficient will be tested and analyzed. The first value ($6\ W/(m^2K)$) will be that of an object in still air, the second value ($500\ W/(m^2K)$) will be the maximum that corresponds to an object in air that is experiencing forced convection and the final value ($1000\ W/(m^2K)$) will correspond to an object submerged in water that is subject to forced convection as well [21]. Based on the temperature response of both the gas and the wall a conclusion will be drawn on the effect of a higher external heat transfer coefficient.

Figure 4.7 shows the wall temperature at the moment the hydrogen supply stops. It can be observed on the outside of the tank, at a wall thickness of 66 mm, the external heat transfer coefficient is a significant factor, but only limited. There is no observable difference between an external transfer coefficient of respectively $500\ W/(m^2K)$ and $1000\ W/(m^2K)$. As the ambient temperature is slightly higher than the initial wall temperature, heat will be added to the outer layer of the tank, which will slowly penetrate the wall of the tank. The limiting factor in this case will be the thermal inertia of the tank wall, which dictates how fast heat can be transferred through the wall. In this case, the convective heat transfer in the tank is limited by the conductance of the wall. A difference in response can be observed when looking at a value of $6\ W/(m^2K)$, but this only results in a difference of $5°C$ with respect to the higher heat transfer coefficients.

The most important conclusion that should be drawn from this is that the gas temperature will not be affected by a higher heat transfer coefficient due to the isolating

properties of the wall. This can be observed in Figure 4.8. The plots for the gas temperature at different external heat transfer coefficients overlap perfectly.

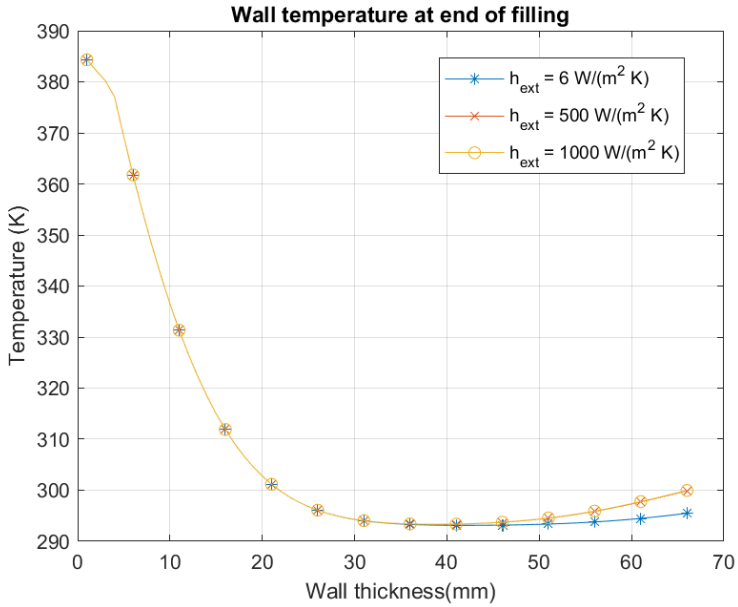

Figure 4.7: Wall temperature at the end of filling, for different external heat transfer coefficients

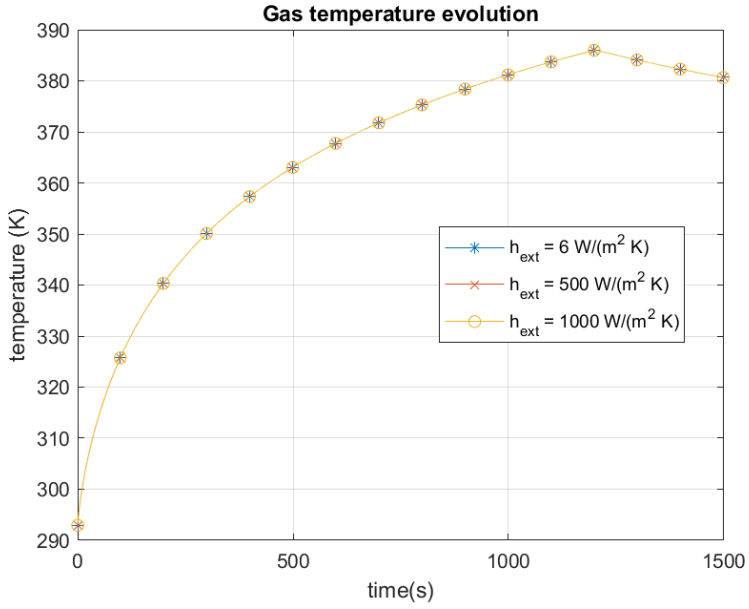

Figure 4.8: Gas temperature evolution for different external heat transfer coefficients

4.5. Conclusion

This chapter is dedicated to the validation of the model and potential improvements. The validation is conducted by comparing the output parameters *mass flow rate* and *compressibility* to experimentally gathered data. Both parameters are in good agreement with the data extracted from the look-up tables.

Furthermore, the transition between materials and the resolution of the wall has been investigated. The value of the expression in this model will remain the same, however, its robustness is updated, to make it feasible for different element sizes to be used if required. From section 4.3 it can be concluded that a resolution of 3 mm does not work well, because the thermal reaction of the liner of the wall cannot be monitored accurately. A resolution of 1 mm in the model fits well and does not differ significantly from a resolution of 0.5 mm in terms of thermal response. Finally section 4.4 describes that the external heat transfer coefficient can indeed be taken at a constant value of $6\ W/(m^2K)$.

5

Parameter study

In chapter 4, the simulation model has been validated and improved. This chapter will focus on how to use the simulation model to assess different input parameters for hydrogen refueling. Two types of parameters can influence the temperature development in the tank: hydrogen-specific parameters and tank-specific parameters.

For the hydrogen-specific parameters, this chapter will discuss the inlet temperature of hydrogen and the pressure ramp rate of the hydrogen in the tank. For the tank-specific parameters, we will explore the liner material and the size of the tank.

It's important to note that we will only consider one variable at a time in each section. The rest of the parameters will remain constant.

By the end of this chapter, we will answer the following sub-question:

How do different input parameters impact the temperature development in the tank during hydrogen refueling?

5.1. Inlet temperature

The temperature of the hydrogen gas entering the tank is of significance to the temperature evolution of the gas in the tank due to the proportional relation between internal energy and temperature ($U = c_v * T$). So the higher the temperature of the incoming gas, the higher the amount of energy supplied to the tank will be. To see the effects of varying the inlet temperature, the gas temperature evolution and the wall temperature at the end of the filling have been plotted in respectively Figure 5.1 and Figure 5.2.
As has been stated above: the higher the inlet temperature, the higher the amount of energy is supplied, which is in agreement with the plots in Figure 5.1 and Figure 5.2 agree with this statement. The influence of cooling the hydrogen before entering the tank is fairly significant on both the maximum temperature and the mass of hydrogen that is refueled, see Table 2. The lower the temperature of the hydrogen, the higher its density becomes, resulting in more mass entering the tank per unit of time. Next to the increased mass flow rate with a lower inlet temperature, the specific enthalpy of the incoming gas (modeled as $c_{p,g}T_{del}$) will decrease as well. Equation 2.5 shows that a reduction in specific enthalpy for the incoming gas will also reduce the internal energy of the system and consequentially the temperature of the gas as well.

Inlet temperature ($^{\circ}C$)	Maximum temperature ($^{\circ}C$)	Mass refueled (kg)
-40	64.4	35.2
-20	81.8	33.6
0	98.4	32.2
20	114.4	31.0

Table 2: Maximum gas temperature and mass refueled for variable inlet temperatures

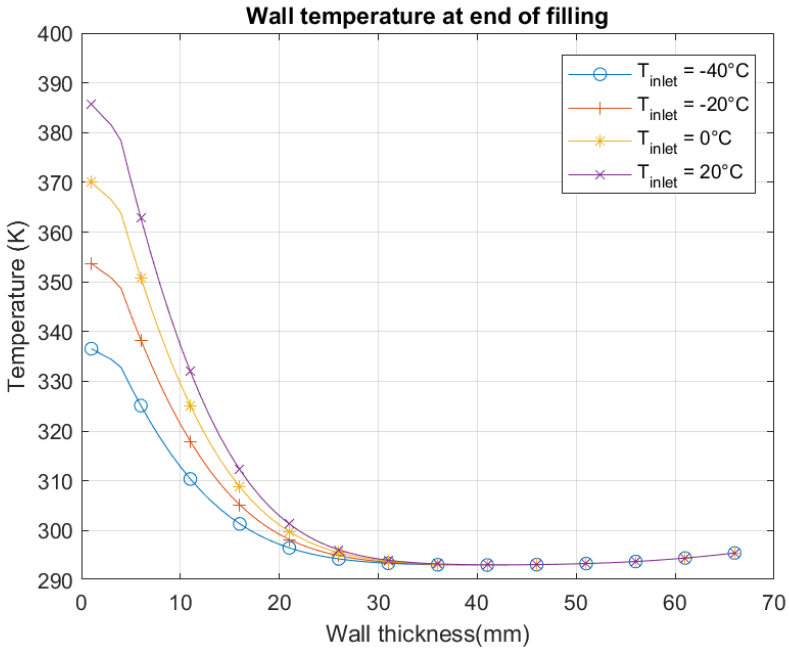

Figure 5.1: Wall temperature at the end of filling, for different inlet temperatures, the dashed green line is the safety limit of the gas temperature

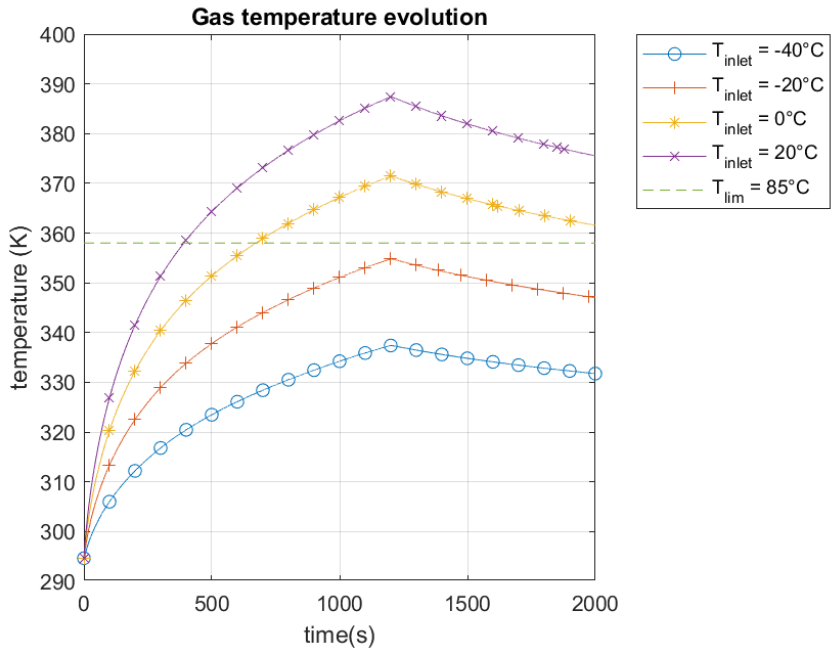

Figure 5.2: Gas temperature evolution for different inlet temperatures

5.2. Pressure Ramp Rate

From Equation 2.4 it follows that the pressure of the gas proportional is to the temperature of the gas. However, due to its interaction with the density, and therefore mass and mass flow rate (Equation 3.1) its evolution is fairly complicated to describe. Equation 2.5 illustrates that the mass flow rate has a positive influence on the internal energy of the gas and consequentially on the gas temperature as well. Figure 5.3 and Figure 5.4 both are in agreement with this statement, where a higher pressure ramp rate means a higher final temperature.
As can be observed in Figure 5.3, a higher temperature is obtained in a shorter period. This higher temperature can be assigned to the conductance of the wall, since there is a limit to the amount of heat that can be conducted away from the gas, per unit of time.

PRR(MPa/s)	Maximum temperature ($^{\circ}C$)	Mass refueled (kg)
0.02	110.0	31.3
0.0275	114.4	31.0
0.035	117.6	30.7

Table 3: Maximum gas temperature and mass refueled for variable pressure ramp rates

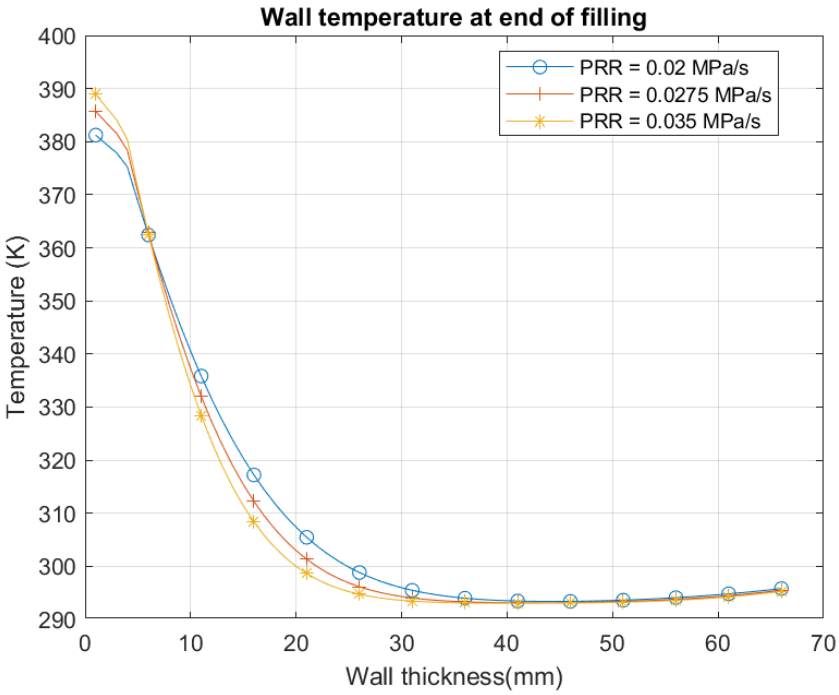

Figure 5.3: Wall temperature at the end of filling, for different pressure ramp rates

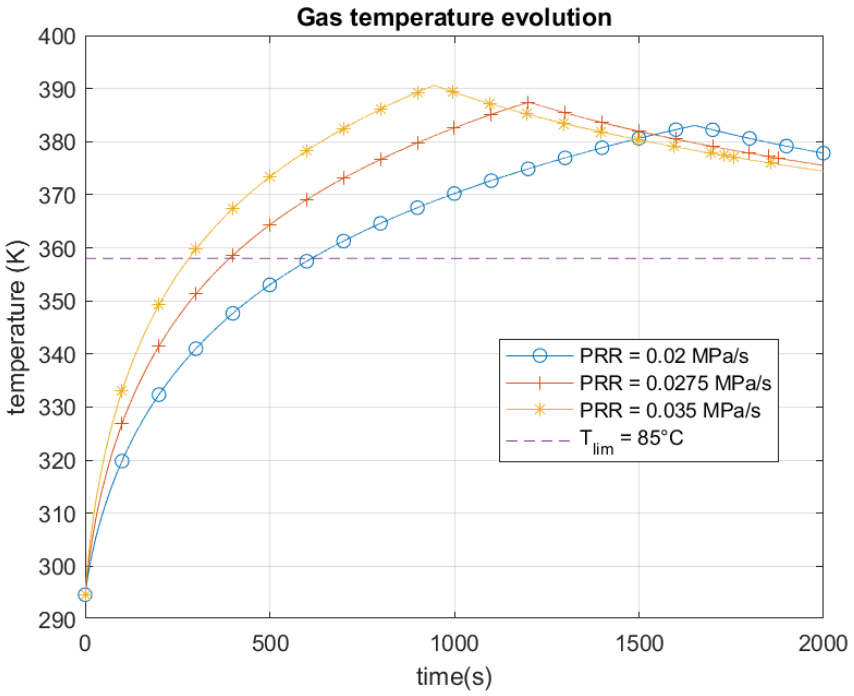

Figure 5.4: Gas temperature at different pressure ramp rates

5.3. Type 3 and Type 4 tanks

The difference between type 3 and type 4 tanks lies in the material of the liner. Where a type 3 tank has a liner made of aluminum, a type 4 tank has a liner mad of polymer.

Quantity	Polymer	Aluminum
Density	$945kg/m^3$	$2698.9kg/m^3$
Conductivity	$0.48W/(mK)$	$210W/(mK)$
Specific heat capacity	$1580J/(kgK)$	$900J/(kgK)$

Table 4: Comparison of the thermal parameters of aluminum and polymer

Type 4 tanks are lighter than type 3 tanks, which would make them slightly more suitable in the use of mobile applications. The material properties of both liner materials can be found in Table 4.

From Table 4 it follows that the conductivity of aluminum is more than 400 times higher than its polymer counterpart. An aluminum liner which is equal in dimensions to a polymer liner has a higher heat capacity (product of ρ_{liner}, $c_{p,liner}$ & V_{liner}). As a consequence, an aluminum liner can store more heat per unit of temperature than a polymer liner. In the case of an aluminum liner, it is expected that the temperature of the liner will nearly be uniform, which is indeed the case, as can be observed in Figure 5.5. This quick conduction of heat combined with a higher heat capacity allows the gas temperature to be lower as well when considering an aluminum liner instead of a polymer liner which can be observed in Figure 5.6.

Tank type	Maximum temperature ($^\circ C$)	Mass refueled (kg)
Type 3	107.6	31.5
Type 4	114.4	31.0

Table 5: Maximum gas temperature and mass refueled for type 3 and type 4 tanks

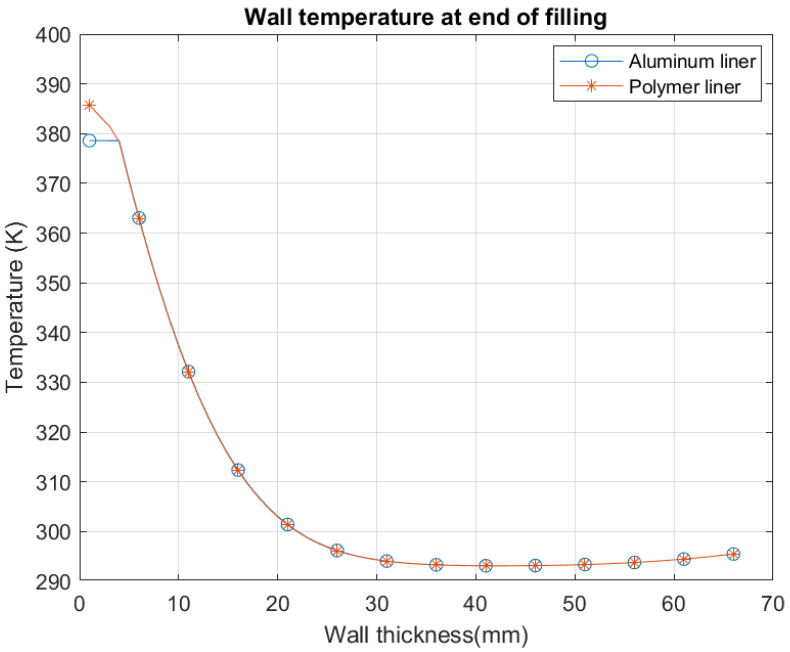

Figure 5.5: Wall temperature at the end of filling, for different liner materials

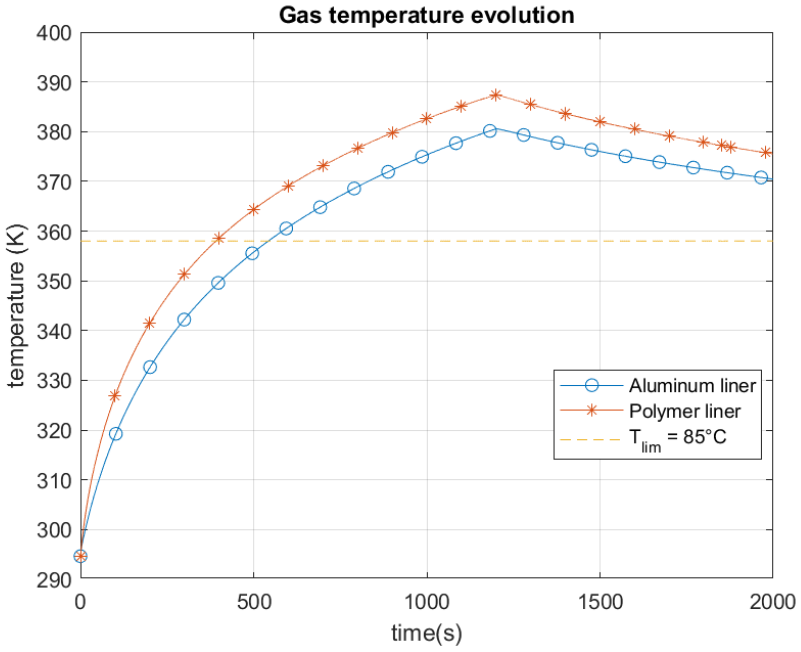

Figure 5.6: Gas temperature for different liner materials

5.4. Tank Volume

The size of a hydrogen tank is of influence on the thermal behavior of the gas. Equation 2.15 shows that an increase in the diameter of the tank will result in a higher Reynolds number, which is associated with increased turbulence of the gas as has been discussed in section 2.2. In this section 4 different tank sizes will be assessed. A diameter of 0.60 m and 0.70 m lie close to the reference value, but the last value, a diameter of 2.5 meters, will be tested to investigate what would happen if one hydrogen tank would completely fit into a 20-foot equivalent unit (TEU) container. The last case is purely conceptual, but it will give insight into why gas tanks of this size will not likely be used. For testing different tank volumes, several assumptions have been made which will be shown in the list below:

- The length of the tank will be kept the same and the diameter of the tank will be the variable. This assumption is made to ensure that the tank will fit in a standard-issue twenty-foot-equivalent unit container (TEU).
- The stress in the wall will be calculated according to the formula for thin-walled pressure vessels: $\sigma = \frac{pr}{t}$, where σ is the stress in the wall, p is the pressure in the tank, r is the radius of the tank (including the wall) and t is the wall thickness. It is important to note that the value of r in the stress formula also includes the thickness of the wall, so with a radius of 0.325m, also the thickness of 0.066m needs to be added [24].
- For all different tank dimensions, the stress in the wall will be assumed to be equal

For the tank that has been considered up until now, a material stress of 217 MPa is present in the wall at a gas pressure of 35MPa. To respect this value, the thickness has to be recomputed for every different tank diameter that will be tested. The different

diameters with their corresponding volumes, thicknesses, and carbon fiber volumes are depicted in Table 6.

Inner diameter	Gas volume	Wall thickness	Carbon fiber volume (m^3)
0.60m	1.5m^3	0.058m	0.66
0.65m	1.8m^3	0.063m	0.77
0.70m	2.1m^3	0.068m	0.90
2.50m	26.6m^3	0.20m	9.22

Table 6: Diameters of the hydrogen tank with corresponding volumes and wall thicknesses

With a larger diameter and consequentially volume, the system changes substantially. Not only is the mass flow rate increased (at equal PRR), but the heat transfer also changes, due to a change in heat transfer parameters (Reynolds number increases) and an increase in surface area, please observe Table 7. This interaction of different factors makes it interesting to see what will happen when increasing or decreasing the size of a tank. From Figure 5.8 it follows that when increasing the tank size, the maximum temperature in the tank will increase as well. In Figure 5.7 it can be observed that the thermal response of the wall is similar in all three cases, despite the difference in thickness. A second plot, Figure 5.7b has been implemented to better observe the response of the tanks with a diameter of respectively 0.6m, 0.65m and 0.7m, since their response is overshadowed by the large wall thickness of the plot corresponding to a diameter of 2.5m.
When increasing the diameter of the tank, the Reynolds number will also increase, as can be observed in Equation 2.15. A higher Reynolds number corresponds to a higher level of turbulence in the tank resulting in a higher heat transfer coefficient. Figure 5.9 is in agreement with the statement above, where it can be observed that an increase in diameter also results in an increase in heat transfer coefficient.
Based on the maximum temperature for each tank, it seems unrealistic to use a single large hydrogen tank. This is due to the high temperature it would generate, which results in a lower density of hydrogen inside the tank. Furthermore, using only one tank takes away redundancy from the system, which means a malfunction in one tank could lead to a complete system failure. On the other hand, using multiple smaller tanks instead of one large tank would be a better approach. In this case, if one tank malfunctions, it won't necessarily result in the failure of the entire system.

Tank diameter (m)	Maximum temperature ($^\circ C$)	Mass refueled (kg)
0.60	111.7	26.5
0.65	114.4	31.0
0.70	116.8	35.7
2.50	149.4	421.9

Table 7: Maximum gas temperature and mass refueled for different tank sizes

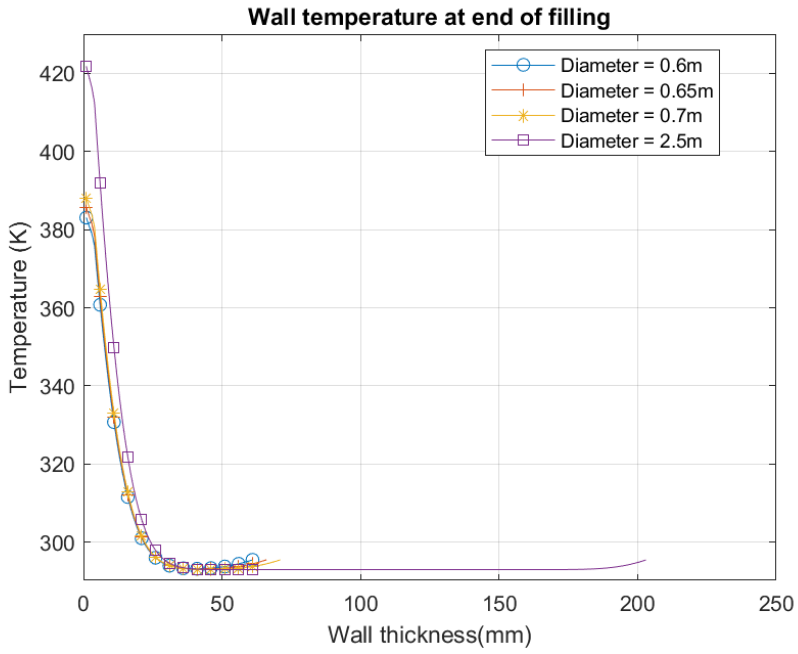

(a) Wall temperature at the end of the filling, including the plot corresponding to a diameter of 2.5 m

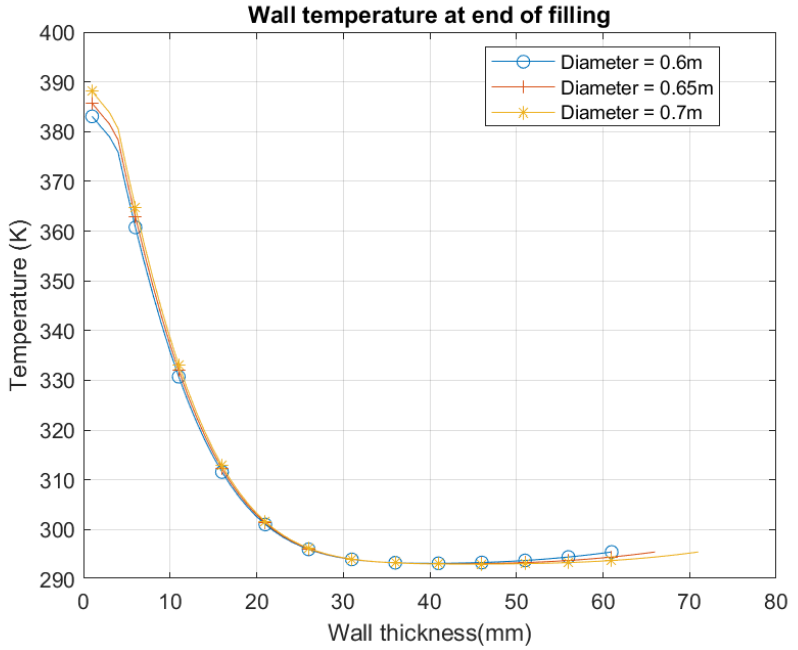

(b) Wall temperature at the end of the filling, excluding the plot corresponding to a diameter of 2.5 m

Figure 5.7: Wall temperature plots, in Figure 5.7b is left out to observe a detailed plot of the wall temperature for tank sizes 0.6m, 0.65m and 0.7m

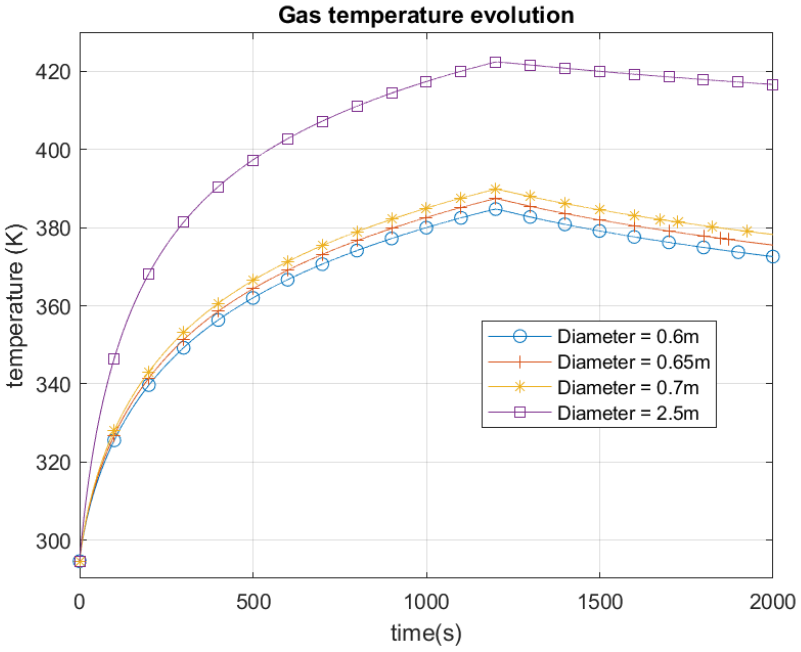

Figure 5.8: Gas temperature for different diameters

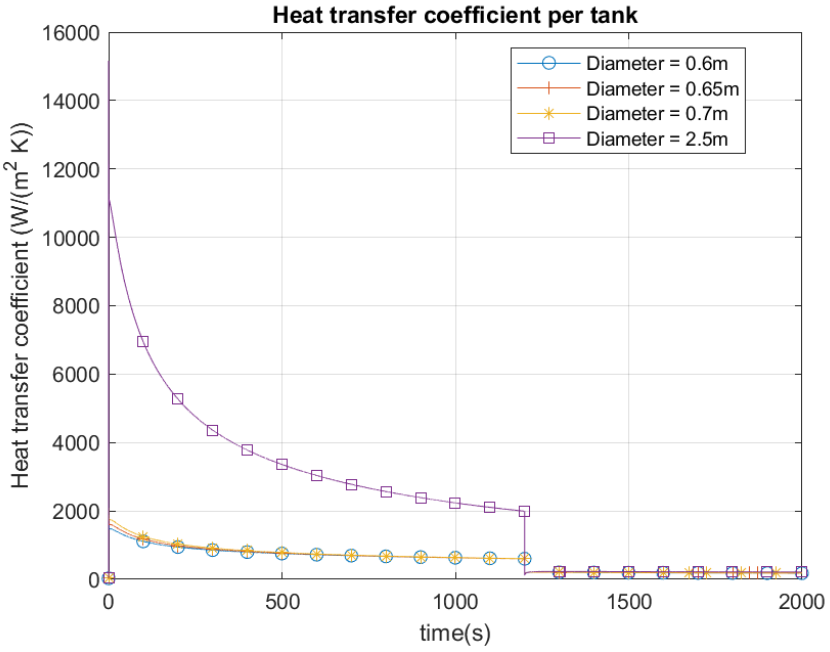

Figure 5.9: Heat transfer coefficient for different diameters

5.5. Feasible combination of input parameters

The previous sections have shown the influence of treating a single parameter as a variable, to get insight into their influence. In the simulation model, all variables have been tested simultaneously to find a feasible combination of input parameters that respects the temperature limit of $85°C$. A feasible combination of parameters is listed

below:

- Tank diameter of $0.7\ m$
- Inlet temperature of $-20\ ^{\circ}C$
- Pressure ramp rate of $0.035\ MPa/s$
- An aluminum liner

This combination will result in a hydrogen temperature of $80.9\ ^{\circ}C$ with a total of $39.1\ kg$ of hydrogen that is refueled. When reducing either the tank diameter, the inlet temperature or the pressure ramp rate a feasible combination will appear as well.

5.6. Conclusion

In this chapter, the variation of several input parameters has been assessed. The gas temperature and the mass of the gas that has been refueled have been used as a KPI due to the inverse relation between the temperature of the gas and its density: the higher the temperature, the lower the density and therefore the lower mass that has been added to the system.
From the results, it follows that reducing the inlet temperature of the gas can be an important factor in making a refueling process feasible shortly. Increasing the pressure ramp rate allows a faster refueling procedure with only a minor loss in the amount of hydrogen that is refueled, however, the temperature limit of 85$^{\circ}C$ has been exceeded significantly.
The desired use of this simulation model has been executed by finding a feasible combination of parameters using the simulation model.

6

Discussion and recommendations

The model that has been developed in this research can give a good insight into the temperature evolution of hydrogen in the tank during refueling. However, it shows room for significant improvement. In this chapter, the shortcomings of the current model will be discussed and a recommendation on the corresponding topic will follow.

The term for the inlet-specific enthalpy that has been used, $c_{p,g}T_{del}$ is not fully representative. This expression is based on the assumption of an ideal gas, but compressibility effects will surface when considering the gas as a real gas. This has been observed when plotting the enthalpy extracted from look-up tables and the ideal gas term for enthalpy, where it comes to attention that the ideal gas enthalpy is substantially (about 10%) higher concerning its real-gas counterpart.

The previous point also builds a bridge to another point of attention. Currently, density and enthalpy are computed using the equations of state and the ideal gas expression for enthalpy. These two values can also be extracted directly from look-up tables, which will significantly reduce the number of equations performed in the simulation, resulting in a clear overview of the calculation process. Another argument for choosing the look-up table values instead of computing them through equations is that the values from look-up tables are established experimentally, and are therefore providing realistic scenarios, as these values reflect actual physical conditions of the gas. It would be recommended to make the model more user-friendly by using the data from look-up tables instead of computing them inside the model.

CFD modeling has shown that for the considered hydrogen tank, in only the first 30% of the tank after the nozzle turbulence occurs, in the residual part of the tank, the hydrogen is relatively at rest. This could indicate that multiple convection regimes are at play inside a tank, which has not yet been considered in fast simulation models. It is well possible that further development of the model from this research can include different convection regimes at different sections of the tank to give a more accurate representation of the behavior of hydrogen in the tank and therefore also in the wall of the tank, which will reduce the offset that is currently apparent. This would require stepping away from the *lumped thermal model*, but when slicing the tank into separate

smaller lumps which will together constitute a complete tank the representative nature of this simulation model can increase.

Another interesting topic to investigate is whether one empirical relation for the dimensionless numbers in the tank (Reynolds, Nusselt, Prandtl) is even possible to set up. It is possible for smaller tanks that have different sizes (up to 150L), but it might be worth investigating if an empirical relation can be set up. Its empirical nature does unfortunately require broad knowledge of how the gas behaves inside the hydrogen tank and in the current situation, the use of large hydrogen tanks is still a relative novelty.

Finally, the computational core of the simulation has been constructed and tested, but it is not user-friendly to use. For increasing the user experience, the use of a graphical user interface (GUI) is advised, in which the input parameters can be entered, after which the simulation model will begin simulating and delivering the required outputs.

7

Conclusion

The goal of this research was to create a fast simulation model to accurately predict the temperature evolution of both the hydrogen gas and the wall of the tank. To achieve this goal, a 0D gas model and a 1D wall model based on existing models have been created, merged and validated. Such a fast simulation tool can help Future Proof Shipping by providing valuable insights into what bunker scenarios can be feasible from a thermodynamic perspective. The research question corresponding to this goal is the following:

How to design a fast simulation tool for a hydrogen tank filling, from which the temperature evolution of both the gas and the tank wall can be observed?

This question is supported by the following sub-questions, which have been answered in their corresponding chapters:

- *What are the theoretical principles behind a hydrogen tank filling?*
- *How is the pressure of the delivered hydrogen controlled?*
- *How does the model perform with respect to the research it is based on?*
- *Are there potential improvements and/or points of interest in the existing model and how should they be addressed?*
- *How do different input parameters impact the temperature development in the tank during hydrogen refueling?*

After the theoretical principles of a hydrogen fill procedure became familiar the simulation model was developed. During validation of the simulation model for a small tank, a substantial positive offset became apparent, whereas the offset for the large tank was smaller. This indicates that further refinement of the model is needed to improve its precision. However, the consistent positive offset suggests a reasonable level of accuracy. Another consequence of this positive offset is the question of whether the model provided by Kesana [7] can already be considered an accurate response, given the fact it is not fully reproducible.

When considering the resolution of the tank wall, it is found that a resolution of 1 mm, gives an accurate response of both the gas temperature and the wall temperature. When investigating the gas-specific parameters (delivery temperature and pressure ramp rate) it has been found that a reduction in gas temperature significantly influences the maximum temperature in the tank. In contrast, a reduction in pressure ramp rate has a smaller reducing effect. Physical changes to the tank itself (changing liner material or changing the volume) influence the evolution of the gas temperature over time and influence the wall temperature as well. When using aluminum as a liner instead of the polymer, heat is transferred through the liner at a much higher rate, also resulting in a lower gas temperature in the tank. This results in a uniform liner temperature whose value lies close to the corresponding gas temperature, contrary to when using a polymer liner. Based on the thermal response, a type 3 tank (with aluminum liner) would be preferable over a type 4 tank (with polymer liner). At last, the response of different volumes has been investigated from which it follows that the volume has a minor positive influence on the maximum temperature of the gas.

To answer the main research question: This research shows the steps that are taken to construct a simulation tool that can depict the temperatures of both the gas and the wall during a filling procedure accurately but not yet precise. Further refinements on this model are required, however, the model is already capable of providing valuable insights into the temperature evolution of both the gas and the wall during a bunker procedure. Using this model, it has been found that when Future Proof Shipping will be bunkering compressed hydrogen for their vessels, it is recommended to keep the inlet temperature $-20^{\circ}C$ or lower and use an aluminum liner when filling a tank with a diameter of $0.7\ m$ at a filling rate of $0.035\ MPa/s$.

Bibliography

1. Shipping, F. P. *Future Proof Shipping* https://futureproofshipping.com/ (2023).
2. Visser, K. *Verduurzaming binnenvaart* tech. rep. (EICB, Marin, TNO, KBN, 2022).
3. Rijksoverheid. *Green Deal on Maritime and Inland Shipping and Ports* 2019.
4. R. Baker, J. Z. *PROTON EXCHANGE MEMBRANE or POLYMER ELECTROLYTE MEMBRANE (PEM) FUEL CELLS* https://knowledge.electrochem.org/encycl/art-f04-fuel-cells-pem.htm (2024).
5. Durbin, D. & Malardier-Jugroot, C. Review of hydrogen storage techniques for on board vehicle applications. *International Journal of Hydrogen Energy* **38,** 14595–14617 (2013).
6. Reddi, K., Elgowainy, A., Rustagi, N. & Gupta, E. Impact of hydrogen SAE J2601 fueling methods on fueling time of light-duty fuel cell electric vehicles. *International Journal of Hydrogen Energy* **42,** 16675–16685 (2017).
7. Kesana, N. R., Welahettige, P., Hansen, P. M., Ulleberg, Ø. & Vågsæther, K. Modelling of fast fueling of pressurized hydrogen tanks for maritime applications. *International Journal of Hydrogen Energy* **48,** 30804–30817 (2023).
8. Tryggvason, G. in *Fluid Mechanics (Sixth Edition)* (eds Kundu, P. K., Cohen, I. M. & Dowling, D. R.) Sixth Edition, 227–291 (Academic Press, Boston, 2016).
9. Moran, N., Shapiro, H., Boettner, D. & Bailey, M. *Principles of Engineering Thermodynamics* (John Wiley & Sons, 2015).
10. Johnston, I. The Noble-Abel Equation of State: Thermodynamic Derivations for Ballistic Modelling (Jan. 2005).
11. Michler, T., Elsässer, C., Wackermann, K. & Schweizer, F. Effect of Hydrogen in Mixed Gases on the Mechanical Properties of Steels—Theoretical Background and Review of Test Results. *Metals* **11** (2021).
12. Kandakure, M., Patkar, V. & Patwardhan, A. Characteristics of turbulent confined jets. *Chemical Engineering and Processing: Process Intensification* **47,** 1234–1245 (2008).
13. Ricou, F. P. & Spalding, D. B. Measurements of entrainment by axisymmetrical turbulent jets. *Journal of Fluid Mechanics* **11,** 21–32 (1961).
14. Molkov, V., Dadashzadeh, M. & Makarov, D. Physical model of onboard hydrogen storage tank thermal behaviour during fuelling. *International Journal of Hydrogen Energy* **44,** 4374–4384 (2019).
15. Cengel, Y. & Ghajar, A. *Heat and mass transfer : a practical approach* (New York: McGraw-Hill, 2010).

16. Gnielinski, V. New equations for heat and mass transfer in the turbulent flow in pipes and channels. *NASA STI/Recon Technical Report A* **41,** 8–16 (Jan. 1975).

17. WOODFIELD, P. L., MONDE, M. & TAKANO, T. Heat Transfer Characteristics for Practical Hydrogen Pressure Vessels Being Filled at High Pressure. *Journal of Thermal Science and Technology* **3,** 241–253 (2008).

18. Barthelemy, H., Weber, M. & Barbier, F. Hydrogen storage: Recent improvements and industrial perspectives. *International Journal of Hydrogen Energy* **42,** 7254–7262 (2017).

19. Cheng, Q., Zhang, R., Shi, Z. & Lin, J. Review of Common Hydrogen Storage Tanks and Current Manufacturing Methods for Aluminium Alloy Tank Liners. *International Journal of Lightweight Materials and Manufacture* (2023).

20. NIST. *NIST Reference Fluid Thermodynamic and Transport Properties Database (REFPROP): Version 8.0* (2023).

21. Kosky, P., Balmer, R., Keat, W. & Wise, G. *Exploring Engineering - An Introduction to Engineering and Design (5th Edition)* (Academic Press, 2021).

22. Klopčič, N. *et al.* Refuelling tests of a hydrogen tank for heavy-duty applications. *International Journal of Hydrogen Energy.* ISSN: 0360-3199 (2023).

23. de Miguel, N. *et al.* The role of initial tank temperature on refuelling of on-board hydrogen tanks. *International Journal of Hydrogen Energy* **41,** 8606–8615 (2016).

24. Hibbeler, R. *Mechanics of Materials* (Pearson, 2014).

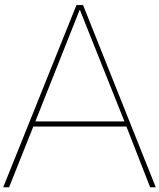

Scientific research paper

Assessing the thermodynamic behavior of bunkering compressed hydrogen for inland cargo vessels

Siebrand Rademaker, *MSc Student, ME TU Delft,*

***Abstract*—A new simulation tool has been developed to provide insights into the refuelling of hydrogen. The tool is based on existing models, consisting of a 0D gas model and a 1D wall model, which have been further refined. The aim of this tool is to help companies, like Future Proof Shipping, who use compressed hydrogen tanks. During the validation process, it was found that the model is not yet fully reproducible and is still subject to changes. However, for large tanks (1500-2100L), the temperature evolution has been computed accurately. Based on this evolution, it has been suggested that it is preferable to maintain the inlet temperature of hydrogen at -20°C or lower. Furthermore, the use of a type 3 hydrogen tank (with an aluminum liner) is recommended for Future Proof Shipping as it has better heat conductivity, allowing heat to be conducted away from the hydrogen more efficiently.**

I. Introduction

Hydrogen, a clean and renewable fuel with zero greenhouse gas emissions, has emerged as a promising alternative for inland cargo shipping, seeking to replace traditional diesel-powered vessels and contribute to a more sustainable future. This is implemented in the *Green Deal on Maritime and Inland Shipping and Ports* with the target to have 150 zero-emission vessels sailing the Dutch inland waterways in 2030 [1]. Hydrogen is used in Proton Exchange Membrane Fuel Cells (PEMFC), where hydrogen is used to create an electrical that drives connected electrical systems, allowing to sail without emitting any greenhouse gasses [2]. *Future Proof Shipping* (FPS) is worldwide the first company that released a 100% emission-free vessel, sailing exclusively on hydrogen.

However, the widespread adoption of hydrogen-powered ships is hindered by the complex challenges associated with hydrogen storage and refueling, particularly for larger tank sizes. The storage of onboard hydrogen is a major challenge due to the limited volumetric energy density of hydrogen compared to conventional fuels such as diesel. To store the same amount of energy, hydrogen stored at 350 bar will occupy a volume that is 10 times as large as that of diesel. The refueling process of hydrogen tanks involves an increase in gas temperature, posing significant safety concerns. To address such concerns efficiently, widespread standards have been introduced that dictate a maximum allowable gas temperature of $85°C$ or $358K$. For companies such as FPS a tool that can compute the temperature evolution of the gas within minutes would be useful to investigate feasible configurations of hydrogen tanks.
The proposed simulation tool is a combined 0D gas model and 1D wall model, however, as little data for refueling large hydrogen tanks ($> 150L$) is available, these models should be based on data extracted from a CFD model. Kesana [3] has used this strategy to construct 0D/1D-model, however, with questionable reproducibility. This issue will be addressed in this research, next to this, the influence of the varying inlet temperature, pressure ramp rate, tank type and tank volume will be addressed. Finally, potential improvements for the model will be identified, as well as recommendations on how these improvements should be implemented.

The developed simulation tool serves as an asset for companies involved in hydrogen storage and refueling operations. By providing insights into the temperature evolution during refueling, the tool enables the optimization of refueling procedures, ensuring safe and efficient operations of hydrogen-powered vessels.

II. Literature study

In this section, the theoretical principles behind a hydrogen fill procedure will be discussed. First, the equations of state for describing the behavior of the hydrogen gas will be discussed. There-after the process of computing the internal heat transfer coefficient will be handled. Finally, the conduction of the heat through the wall will be discussed.

A. Thermodynamics

The behavior of the gas will be described by using the *Abel-Noble* equations of state [4], [5]:

$$P(v - b) = R_{H_2}T \tag{1}$$

Where P is the pressure in the system, v is the specific volume of the gas, b is the factor that takes the finite volume of molecules into account, R_{H_2} is the hydrogen-specific gas constant and T is the temperature of the gas. When isolating T from Equation 1 and substituting v with $\frac{1}{\rho}$ the following equation will emerge:

$$T = \frac{P(1 - b\rho)}{\rho_{gas}R_{H_2}} \tag{2}$$

where ρ_{gas} is the density of the gas. The relation $U = c_vT$ is used to relate the temperature and internal energy. The first law of thermodynamics describes an energy balance between the incoming and outgoing energy from the gas. Its expression is as follows [6], [7]:

$$\frac{dU}{dt} = \frac{dQ}{dt} + h_{in}\dot{m}_{gas} \tag{3}$$

Where $\frac{dU}{dt}$ is the change of internal energy of the gas, $\frac{dQ}{dt}$ is heat added to/subtracted from the gas, $\dot{m}_{gas}$ is the mass flow of the gas in the tank and h_{in} is the enthalpy of the incoming gas. In the case of the hydrogen, the heat added to/subtracted is described according to the following expression [8]:

$$\frac{dQ}{dt} = h_{int} A_{int} (T_{wall,int} - T_{gas}) \tag{4}$$

Where h_{int} is the internal convective heat transfer coefficient, A_{int} is the internal surface area of the tank, $T_{wall,int}$ is the internal wall temperature and T_{gas} is the temperature of the hydrogen gas.

B. Convective heat transfer

The value of h_{int} depends on the convection regime that is present in the tank. If the gas in the tank is in turbulent motion, forced convection is in play, whereas stationary motion of the gas indicates natural convection to be present. To determine which convection regime and its corresponding heat transfer coefficient is present, selection criteria that are based on the Reynolds number and the Grashof number have been established, they are shown in Equation 7.
The Grashof number is a ratio between buoyancy effects and viscous effects in the tank [9]:

$$Gr_{tank} = \frac{g\alpha |T_{gas} - T_{wall,int}| \rho_{gas}^2 D_{int}^3}{\mu_{gas}^2} \tag{5}$$

where g is the gravitational constant, ρ_{gas} is the density of the gas, D_{int} is the internal diameter of the tank and μ_{gas} is the dynamic viscosity of the gas.
The *Reynolds*-number is a ratio between inertial effects and viscous effects in the gas, with an increasing Reynolds number, the turbulent motion of the gas also becomes more apparent. The characteristic Reynolds number in the tank is calculated as follows [9]:

$$Re_{tank} = \frac{\rho_{gas} u_{tank} D_{int}}{\mu_{gas}} \tag{6}$$

where u_{tank} is a characteristic velocity of the hydrogen in the tank. This value will be explained in detail after Equation 7. Furthermore, D_{int} is the internal diameter of the tank and μ_{gas} is the dynamic viscosity of the hydrogen in the tank.

$$\begin{cases} \text{if } \frac{Gr_{tank}}{(Re_{tank})^2} < 0.1,\ h_{int} = h_{int,forced} \\ \text{if } 0.1 < \frac{Gr_{tank}}{(Re_{tank})^2} < 10,\ h_{int} = (h_{int,natural}^4 + h_{int,forced}^4)^{\frac{1}{4}} \\ \text{if } \frac{Gr_{tank}}{(Re_{tank})^2} > 10,\ h_{int} = h_{int,natural} \end{cases} \tag{7}$$

where the Gr_{tank} is the *Grashof*-number in the tank and Re_{tank} is the *Reynolds*-number in the tank.

The characteristic velocity, u_{tank}, that is used in Equation 6 is a value which is used to compute the Reynolds number for a complete tank. Its derivation originates from the total kinetic energy of the hydrogen in the tank, which is the sum of the kinetic energy of the inlet hydrogen and that of the hydrogen which is entrained by the jet stream of the incoming gas, see Equation 8 [8]:

$$\frac{m_{gas}(u_{tank})^2}{2} = \frac{m_{ent}(u_{ent})^2}{2} + \frac{m_{inlet}(u_{inlet})^2}{2} \tag{8}$$

where m_{gas} is the mass of the gas in the tank, u_{tank} is the characteristic velocity of the gas in the tank, m_{ent} is the entrainment mass, u_{ent} is the entrainment velocity, m_{inlet} is the inlet mass which is calculated by taking the product of the inlet mass flow rate and the time-step of the simulation, and u_{inlet} is the inlet velocity of the gas.
In this expression for the kinetic energy of the gas, the entrainment mass of the gas is assumed to be equal to the mass of the gas in the tank. For smaller tanks, this assumption can be considered as valid as all gas in the tank participates in the turbulent behavior. However, when increasing the size of the tank, a portion of the gas in the tank will become stagnant, which will induce a difference between m_{tank} and m_{ent}.

The entrainment process increases the mass flow rate of the jet, and the characteristic velocity of the hydrogen is calculated by considering the kinetic energy of the inlet velocity and the entrainment velocity. The entrainment velocity is determined using the inlet velocity u_{inlet} (Equation 9), the momentum flux of the incoming hydrogen M_0 (Equation 10) and the entrainment mass flow rate $\dot{m}_{ent}$ (Equation 11). When the mass flow rate is known, the velocity of a fluid flowing through a body with a circular cross-section can be calculated according to Equation 12 [8], [10]:

$$u_{inlet} = \frac{4\dot{m}_{gas}}{\rho_{gas}(D_{inlet})^2 \pi} \tag{9}$$

$$M_0 = \frac{1}{4}\pi (D_{inlet})^2 \rho_{inlet} (u_{inlet})^2 \tag{10}$$

$$\dot{m}_{ent} = 0.282 (M_0)^{0.5} (\rho_{gas})^{0.5} L \tag{11}$$

$$u_{ent} = \frac{4\dot{m}_{ent}}{\rho_{gas}(D_{int})^2 \pi} \tag{12}$$

The internal heat transfer coefficient is included in Equation 7. Its value can either be computed according toEquation 13 [9]:

$$h_{int} = \frac{k_{gas} Nu_{int}}{D_{int}} \tag{13}$$

where k_{gas} is the conductivity of the gas and Nu_{int} is the *Nusselt*-number of the gas. The Nusselt number can either correspond to forced convection or natural convection. When forced convection is the dominant regime, the Nusselt number becomes a function of the Reynolds number (Re_{tank}), the Prandtl number (Pr) and the friction factor (f) [9], [11]:

$$Nu_{int,forced} = \frac{(f/8)(Re_{tank} - 1000)Pr}{1 + 12.7(f/8)^{0.5}(Pr^{2/3} - 1)} \tag{14}$$

The validity of Equation 14 holds under the following conditions:

$$\begin{cases} 0.5 \leq Pr \leq 2000 \\ \\ 3 * 10^3 < Re < 5 * 10^6 \end{cases} \tag{15}$$

The Prandtl number describes the thickness of the thermal boundary layer. It is computed as follows:

$$Pr = \frac{\mu_{gas} c_{p,gas}}{k_{gas}} \tag{16}$$

The friction factor of the gas is a dimensionless parameter related to the shear stress in the gas. Due to the smooth nature of the wall inside the tank, the following expression for the friction factor will be used:

$$f = \frac{1}{(0.790 ln(Re_{tank}) - 1.64)^2} \tag{17}$$

Natural convection is, in contrast to forced convection, a passive type of convection, where the *Nusselt*-number is based on buoyancy effects that occur due to local temperature (and therefore density) variations in the gas. An equation of the *Nusselt*-number in hydrogen applications has been established [9], [12]:

$$Nu_{int,nat} = 0.104 \left(\frac{g\alpha |T_{gas} - T_{wall,int}| c_{p,gas} (\rho_{gas})^2 D_{int}^3}{\mu_{gas} k_{gas}} \right)^{0.352} \tag{18}$$

A common parameter used to quantify natural convection is the *Rayleigh*-number, which is the product of the *Grashof*- and the *Prandtl* number. The term between brackets in Equation 18 is the Rayleigh number.

C. Conductive heat transfer

The correct wall temperature is essential to compute the correct gas temperature as well. An increase in gas temperature has an increase in the wall temperature as a consequence. The heat will be distributed through a material by conduction. Heat conduction through the wall is described according to the following formula:

$$\rho_{wall} c_{p,wall} \frac{dT_{wall}}{dt} = \frac{d}{dx} \left(k_{wall} \frac{dT_{wall}}{dx} \right) \tag{19}$$

Where ρ_{wall} is the density of wall material, $c_{p,wall}$ the specific heat capacity of the wall material, $\frac{dT_{wall}}{dt}$ the temperature evolution of the wall over time, k_{wall} the conductivity of the wall material and $\frac{dT_{wall}}{dx}$ the temperature evolution of the wall over the width of the wall.

III. Methodology

The theoretical principles that are introduced in section II will in this section be coupled to the simulation model, which is in its core based on the model provided by Kesana [3]. subsection III-A will introduce the simulation software and the type of simulation, and subsection III-B will describe the post-processing of the theory from section II to make this ready to use in the simulation model.

Parameter	Base model value
Pressure Ramp Rate (PRR)	$0.0275\ MPa/s$
gravitational constant (g)	$9.81\ m/s^2$
Initial gas pressure in tank (P_{ini})	$2\ MPa$
Tank volume (V)	$1.8\ m^3$
Tank diameter (D_{int})	$0.65\ m$
Tank length (L_{tank})	$5.42\ m$
Nozzle diameter (D_{inlet})	$0.004\ m$
Initial wall temperature ($T_{wall,ini}$)	$293\ K$
Initial gas temperature ($T_{gas,ini}$)	$293\ K$
Ambient temperature (T_{amb})	$300\ K$
Gas delivery temperature (T_{del})	$293\ K$
Liner density (ρ_{liner})	$945\ kg/m^3$
Liner specific heat capacity ($c_{p,liner}$)	$1580\ J/(kgK)$
Liner conductivity (k_{liner})	$0.48\ W/(mK)$
Liner element size (Δx_L)	$0.001\ m$
Fiber density (ρ_{fiber})	$2051\ kg/m^3$
Fiber heat capacity ($c_{p,fiber}$)	$878\ J/(kgK)$
Fiber conductivity (k_{fiber})	$0.113\ W/(mK)$
Fiber element size (Δx_c)	$0.001\ m$
External heat transfer coefficient (h_{ext})	$6\ W/(m^2K)$

TABLE I
INPUT PARAMETERS OF THE SIMULATION MODEL

A. Simulation model

To limit the computational effort, a lumped-gas model is selected to represent the gas in the simulation (0D), combined with a 1D wall model. As the thermodynamics of the hydrogen tank are only subject to small changes in equilibrium (hydrogen supply and heat exchange), a quasi-static approach in the modeling will be used [6]. The quasi-static nature of the model allows to extract steady-state values (as a function of temperature and pressure) from look-up tables. The values that will be used in the simulation are the specific heat capacity of the gas ($c_{p,gas}$, the dynamic viscosity of the gas (μ_{gas}) and the thermal conductivity of the gas (k_{gas}). The values in these look-up tables are experimentally established by the NIST and can therefore be considered as real-world effects [13].
The input parameters for the simulation model are listed in Table I. Note that the external heat transfer coefficient is assumed to be a constant value, this assumption will be validated in section IV.

A schematic depiction of the full calculation process is provided in Figure 1. In this calculation scheme, the loop of values that is computed every time-step again is located within the dotted line.

B. Post processing of the literature

This subsection will be dedicated to introducing the expressions for mass flow rate and the temperature response for the wall.

a) Mass flow rate: The mass flow rate is computed by combining the Abel-Noble equations of state and the first law of thermodynamics. After substituting the Abel-Noble equations in the expression for the first law, the mass flow rate is isolated and the following expression is obtained [8]:

$$\frac{dm_{gas}}{dt} = \frac{\frac{dP_{gas}}{dt}\frac{(V-m_{gas}*b)}{\gamma-1} - h_{int} * A_{int}(T_{wall,int} - T_{gas})}{\frac{P_{gas}}{\gamma-1} * b + c_{p,gas}T_{del}} \tag{20}$$

b) Wall temperature: During simulation, the wall of the tank is divided into a finite amount of elements, each transferring heat to the next element. The wall of the tank is made up of a liner section (this layer prevents the ingress of hydrogen molecules in the wall) and a fiber section (this layer represents the stress-bearing part of the tank). Since it is made up of two different materials, the thermal response of these materials is also different. The first (inner-most) and the last element (outer-most) are subject to convection. However, the other elements in the wall are subject to conduction at different rates in the different layers. Conduction between the last element of the liner and the first element of the fiber part will take place at the average rate of both parts. A simplified depiction of the heat transfer process can be visualized using a resistance scheme, where each separate type of heat transfer has its own resistance. The scheme corresponding to the tank wall can be observed in Figure 4.

IV. Validation

This section will validate the model on a few levels. First, the mass flow rate and the compressibility that are computed using the Abel-Noble equations of state will be compared to their counterpart that are extracted from look-up tables. Second, the temperature evolution of the simulation model will be compared to the results that are generated by Kesana [3]. Next to this, the simulation model will be adjusted so that it corresponds to a tank of 29L instead of 1800L. The results of this adjustment will be compared to the corresponding results as provided by DeMiguel [14]. Finally, the optimal resolution for the wall model will be determined by observing the temperature response of separate resolutions.

A. Mass flow rate and compressibility

a) Mass flow rate: The mass flow rate in the model is computed according to Equation 20. The mass flow rate that is based on the look-up tables is computed according to the following equation:

$$\dot{m}_{gas} = \dot{\rho}_{gas} * V \tag{21}$$

where $\dot{m}_{gas}$ is the mass flow rate of the gas entering the tank, $\dot{\rho}_{gas}$ is the rate of change of the density of the gas in the tank and V is the volume of the tank. The relation in Equation 21 will be valid until the hydrogen supply is cut off. After this point, the density changes due to temperature variations, but not because of mass entering or leaving the system.
Figure 2 shows agreement between the mass flow to both methods of computation.

b) Compressibility: The term for compressibility can be found in Equation 1. When isolated it read the following:

$$\frac{1}{1 - b\rho_{gas}} \tag{22}$$

This term is compared to the compressibility that is provided by the look-up tables, as can be observed in Figure 3. Agreement in this figure can be observed as well, as the plots do not deviate more than 2% from each other.

B. Temperature evolution

An important measure of this research is the temperature evolution of the gas. In this part, the temperature evolution of the developed model will be compared to the temperature of the model it is based on [3]. The developed model,Figure 5, and the model by Kesana, Figure 6, show good agreement in final temperature (respectively $108°C$ vs. $113°C$). Close observation reveals that the curve from the developed model is slightly less steep than that of the model from Kesana.

To further validate the model, the inputs of the simulation model have been set to a tank with a volume of 29L. This has been compared to its counterpart, provided by DeMiguel [14]. The difference between the maximum temperature of the models of a 29L-tank is substantially bigger. This raises a question on the reproducible nature of the model provided by Kesana. A shortcoming of the lumped-gas modeling is that the complete volume of gas is considered as a single lump. This shortcoming can be observed when looking at the results for the CFD-model provided by Kesana, where it follows that only in the first 28% of the tank hydrogen circulates, which would indicate that natural convection should be the leading regime in the rest of the 72% of the tank. It is considered likely that the heat transfer for the large tank is over-estimated, and therefore the temperature is under-estimated. However, the shape of the curves from both the other two researches and the developed model shows agreement. Keeping this observation in mind, the research will be continued.

C. Wall resolution

Until this point, the elements of the wall each had a size of $\Delta x = 0.001m$. The influence of this element size should be investigated, as a higher resolution also requires more computational effort in the simulation. To investigate the effects of using different resolutions in the simulation model, 3 different wall element sizes have been compared to each other: 0.5 mm, 1 mm and 3 mm. An element size of 3 mm is a special case, as this would result in only a single element for the liner. It has been found that the temperature response of the gas is for all different element sizes nearly identical. The wall temperature for element sizes 0.5 mm and 1 mm is nearly identical, but the wall temperature of an element size of 3 mm is depicted poorly, as can be observed in Figure 9.

An additional observation of the temperature of the tank wall is that its thermal inertia is fairly high. At a thickness of 40mm, the temperature of the wall is still the same as it was at the start of the simulation.

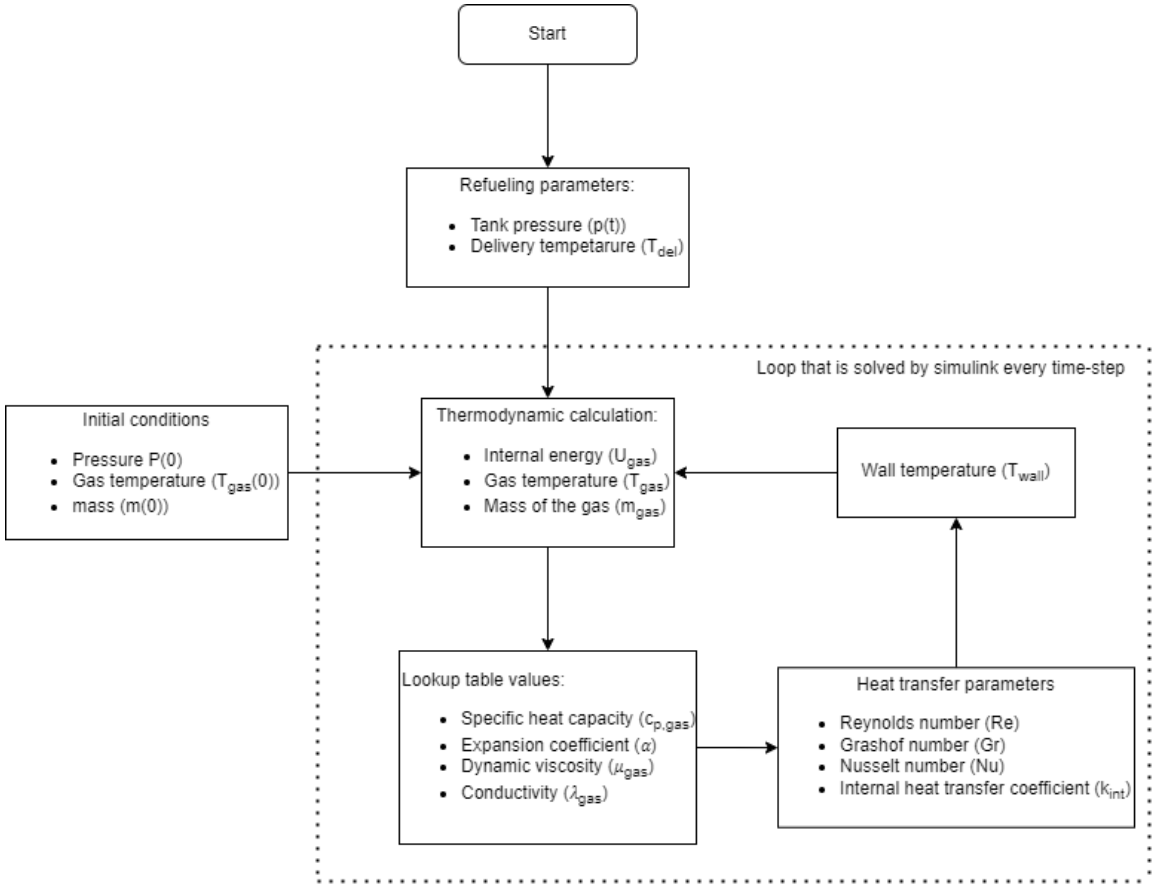

Fig. 1. Schematic overview of the calculation process for every time-step

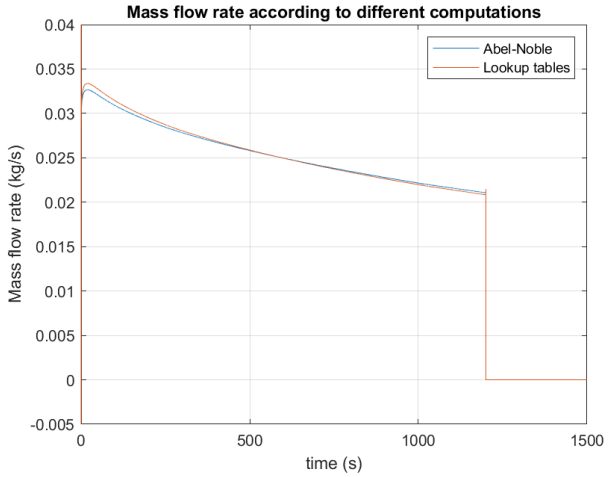

Fig. 2. Computation of $\dot{m}$ according to both the *Abel-Noble* gas model and look-up tables

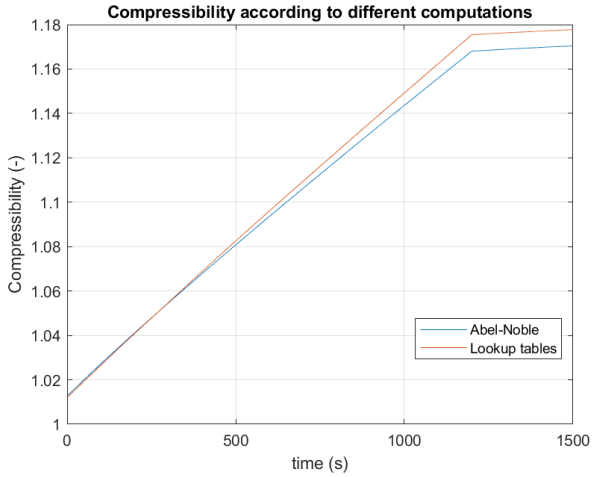

Fig. 3. Computation the compressibility according to both the *Abel-Noble* gas model and look-up tables

D. Heat transfer coefficient

In the input parameters that are discussed in subsection III-A, the external heat transfer coefficient is considered to be a constant value of $6W/(m^2K)$. To validate this assumption, the temperature response of the wall for different heat transfer coefficients has been compared. For the different values for the heat transfer coefficient, a value for an object in still air ($6W/(m^2K)$), a value for an object in turbulent air ($500W/(m^2K)$) and a value for an object submerged in turbulent water flow ($1000W/(m^2K)$) has been selected [15]. The temperature evolution can be observed in Figure 10. It follows that the external wall temperature evolution only

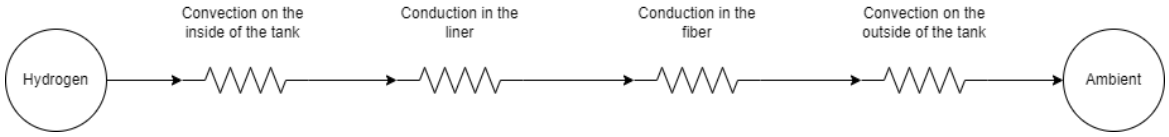

Fig. 4. Schematic overview of the different resistances of the wall

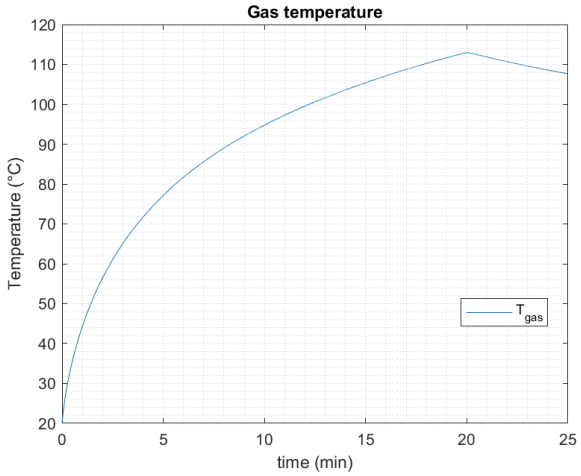

Fig. 5. Computation of $\dot{m}$ according to both the *Abel-Noble* gas model and look-up tables

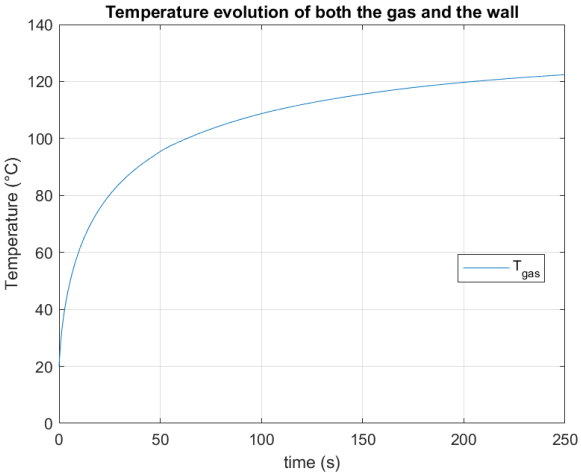

Fig. 7. Temperature evolution of a 29L hydrogen tank filling, as computed by the developed model

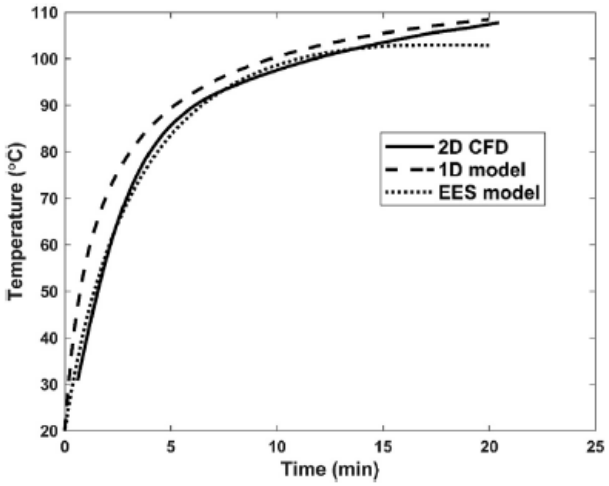

Fig. 6. Computation of $\dot{m}$ according to both the *Abel-Noble* gas model and look-up tables

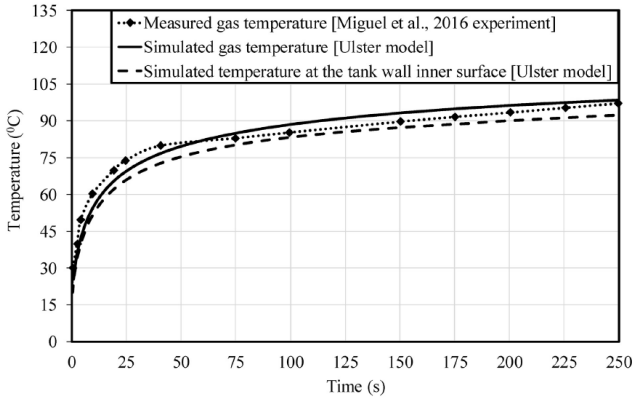

Fig. 8. Temperature evolution of a 29L hydrogen tank filling obtained by De Miguel [14]

influences the outer part of the tank and that the temperature response of the inner part of the tank is nearly identical. The same applies to the hydrogen temperature, which is also identical.

V. Parameter Study

This section will aimed using the developed model to investigate the response to varying the following parameters: Inlet temperature, Pressure ramp rate, Tank type (3 & 4), and tank volume. In each paragraph, the variation of a single parameter will be discussed. Finally, a feasible combination of several parameters will be established. The KPI's corresponding to the variable parameters will be the final temperature and the mass of hydrogen that is refueled.

A. Inlet temperature

As there is a positive relation between the temperature and the internal energy of a gas, it can be derived that a higher inlet temperature will also increase the total gas temperature in the tank. This relation is confirmed when observing the results of the simulation, where a higher inlet temperature also results in a higher gas temperature. A higher gas temperature means a lower gas density, which can also be seen in the mass that is refueled. For a higher inlet temperature, less mass of hydrogen

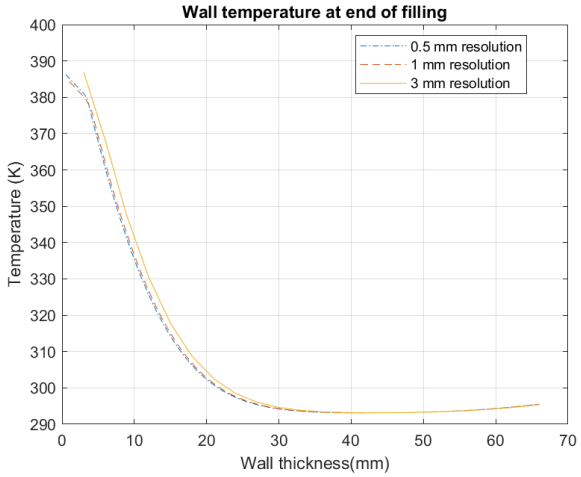

Fig. 9. Wall temperature at the end of filling for different resolutions

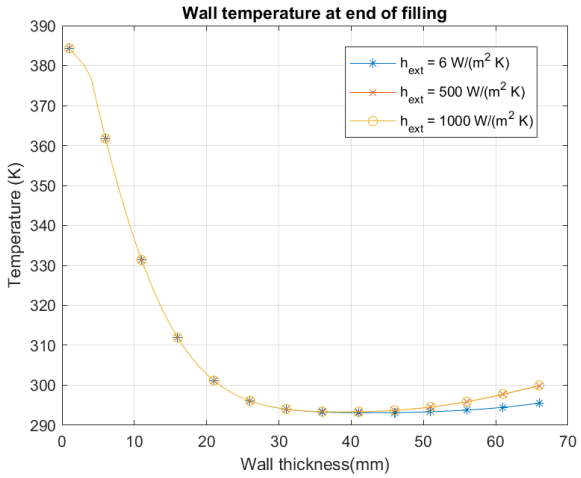

Fig. 10. Wall temperature at the end of filling for different heat transfer coefficients

is added to the system. It follows that the inlet temperature can be considered as a crucial parameter, since an inlet temperature of $-20°C$ or lower will keep the gas temperature below its safety limit. The KPI's of varying the inlet temperature are put in Table II.

T_{inlet} $(°C)$	Maximum temperature $(°C)$	Mass refueled (kg)
-40	64.4	35.2
-20	81.8	33.6
0	98.4	32.2
20	114.4	31.0

TABLE II
MAXIMUM GAS TEMPERATURE AND MASS REFUELED FOR VARIABLE INLET TEMPERATURES

B. Pressure Ramp Rate

The higher the pressure ramp rate, the sooner the target pressure is reached. However this also reduces the amount of heat that can be transferred away from the gas, due to the high

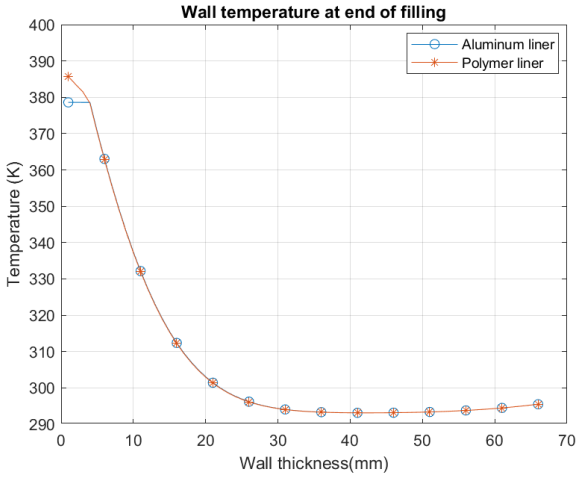

Fig. 11. Wall temperature at the end of filling, for different liner materials

thermal inertia of the wall. Table III shows that the temperature of the gas is slightly higher for a faster pressure ramp rate, where the total refueled mass is slightly lower in the end.

PRR(MPa/s)	Maximum temperature $(°C)$	Mass refueled (kg)
0.02	110.0	31.3
0.0275	114.4	31.0
0.035	117.6	30.7

TABLE III
MAXIMUM GAS TEMPERATURE AND MASS REFUELED FOR VARIABLE PRESSURE RAMP RATES

C. Type 3 and type 4 tanks

The difference between type 3 and type 4 tanks lies in the material of the liner. Where a type 3 tank has a liner made of aluminum, the liner of a type 4 tank is made of a lighter polymer. Polymer, however, has a far lower thermal conductivity, meaning that its isolating properties are better than that of aluminum. The isolating properties can be observed in Figure 11. Where there is a significant difference between the inner polymer element and the outer polymer element, the temperature throughout the aluminum liner is nearly uniform. Because aluminum can transfer heat at a much higher rate, the final gas temperature will also be lower when using a type 3 tank instead of a type 4 tank. This can be observed in Table IV.

Tank type	Maximum temperature $(°C)$	Mass refueled (kg)
Type 3	107.6	31.5
Type 4	114.4	31.0

TABLE IV
MAXIMUM GAS TEMPERATURE AND MASS REFUELED FOR TYPE 3 AND TYPE 4 TANKS

D. Tank Volume

The volume of the tank is influential in the evolution of the temperature. To observe these influences, the model has

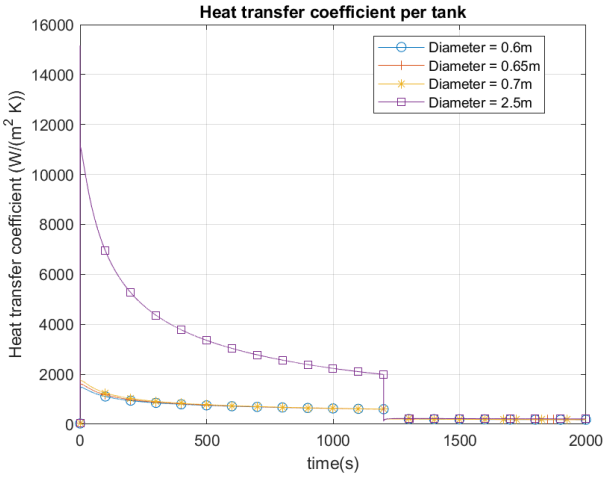

Fig. 12. Heat transfer coefficient for different diameters

Tank diameter (m)	Maximum temperature ($°C$)	Mass refueled (kg)
0.60	111.7	26.5
0.65	114.4	31.0
0.70	116.8	35.7
2.50	149.4	421.9

TABLE V
MAXIMUM GAS TEMPERATURE AND MASS REFUELED FOR DIFFERENT TANK SIZES

been adjusted accordingly to suit the different tank diameters: 0.6 m, 0.65m, 0.7m and 2.5m. The large tank diameter is also considered to investigate the feasibility of using just one hydrogen tank instead of multiple smaller tanks. Upon varying the diameter, the wall thicknesses are also updated in such a fashion that the maximum stress in the wall for each different diameter will remain equal [16]. An increase in diameter will increase the Reynolds number as well, observe Equation 6. From this observation, it can follow that forced convection will apply and that the corresponding transfer coefficient will also increase. This is confirmed in Figure 12, where it can be observed that at an increasing diameter, the heat transfer coefficient increases as well, though for small differences in diameter only slightly, but a diameter of 2.5 m is paired with an enormous heat transfer coefficient due to its increased turbulence.

Despite the substantial increase in diameter, from Table V it follows that the maximum temperature that is present in the tank for a diameter of 2.5m is still significantly higher than the other dimensions. Their diameters were kept close, and this is the case for the maximum temperature as well. However, when refueling at the same pressure ramp rate, it can also be concluded that only a slight increase in diameter (5 cm) can already result in a much higher capacity of a single hydrogen tank, whereas the increase in temperature is only $5°C$.

E. Feasible combinations

Based on the parameter study, a feasible combination of input parameters has been established with the following values:

- Tank diameter of 0.7 m
- Inlet temperature of $-20°C$
- Pressure Ramp Rate of $0.035MPa/s$
- An aluminum liner

This combination will result in a hydrogen temperature of $80.9\ °C$ with a total of $39.1\ kg$ of hydrogen that is refueled. When reducing either the tank diameter, the inlet temperature or the pressure ramp rate a feasible combination will appear as well.

VI. Discussion

The research developed a model for the temperature evolution of hydrogen but it needs significant improvement. The inlet-specific enthalpy term used is not fully representative, and the density and enthalpy can be extracted from look-up tables to make the model more user-friendly. The model needs to consider different convection regimes at different sections of the tank to give a more accurate representation of the behavior of hydrogen. It is also worth investigating if an empirical relation can be set up for dimensionless numbers in the tank. Lastly, a graphical user interface (GUI) is advised to increase the user experience.

VII. Conclusion

This research created a simulation tool to predict the temperature of both hydrogen gas and tank walls during filling. The tool merges a 0D gas model and a 1D wall model, validated for accuracy, but not yet precision. Results show that an aluminum liner and lower gas temperature are favorable for bunkering compressed hydrogen. The model needs further refinement but already provides valuable insights for Future Proof Shipping.

References

[1] Rijksoverheid, “Green deal on maritime and inland shipping and ports,” 2019.
[2] J. Z. R. Baker. Proton exchange membrane or polymer electrolyte membrane (pem) fuel cells. [Online]. Available: https://knowledge.electrochem.org/encycl/art-f04-fuel-cells-pem.htm
[3] N. R. Kesana, P. Welahettige, P. M. Hansen, Øystein Ulleberg, and K. Vågsæther, “Modelling of fast fueling of pressurized hydrogen tanks for maritime applications,” *International Journal of Hydrogen Energy*, vol. 48, no. 79, pp. 30 804–30 817, 2023.
[4] I. Johnston, “The noble-abel equation of state: Thermodynamic derivations for ballistic modelling,” 01 2005.
[5] T. Michler, C. Elsässer, K. Wackermann, and F. Schweizer, “Effect of hydrogen in mixed gases on the mechanical properties of steels—theoretical background and review of test results,” *Metals*, vol. 11, no. 11, 2021.
[6] N. Moran, H. Shapiro, D. Boettner, and M. Bailey, *Principles of Engineering Thermodynamics*. John Wiley & Sons, 2015.
[7] T. Bourgeois, F. Ammouri, D. Baraldi, and P. Moretto, “The temperature evolution in compressed gas filling processes: A review,” *International Journal of Hydrogen Energy*, vol. 43, no. 4, pp. 2268–2292, 2018.
[8] V. Molkov, M. Dadashzadeh, and D. Makarov, “Physical model of onboard hydrogen storage tank thermal behaviour during fuelling,” *International Journal of Hydrogen Energy*, vol. 44, no. 8, pp. 4374–4384, 2019.
[9] Y. Cengel and A. Ghajar, *Heat and mass transfer : a practical approach*. New York: McGraw-Hill, 2010.
[10] F. P. Ricou and D. B. Spalding, “Measurements of entrainment by axisymmetrical turbulent jets,” *Journal of Fluid Mechanics*, vol. 11, no. 1, p. 21–32, 1961.
[11] V. Gnielinski, “New equations for heat and mass transfer in the turbulent flow in pipes and channels,” *NASA STI/Recon Technical Report A*, vol. 41, no. 1, pp. 8–16, Jan. 1975.

[12] P. L. WOODFIELD, M. MONDE, and T. TAKANO, "Heat transfer characteristics for practical hydrogen pressure vessels being filled at high pressure," *Journal of Thermal Science and Technology*, vol. 3, no. 2, pp. 241–253, 2008.

[13] NIST. Nist reference fluid thermodynamic and transport properties database (refprop): Version 8.0.

[14] N. de Miguel, B. Acosta, D. Baraldi, R. Melideo, R. Ortiz Cebolla, and P. Moretto, "The role of initial tank temperature on refuelling of on-board hydrogen tanks," *International Journal of Hydrogen Energy*, vol. 41, no. 20, pp. 8606–8615, 2016.

[15] P. Kosky, R. Balmer, W. Keat, and G. Wise, *Exploring Engineering - An Introduction to Engineering and Design (5th Edition)*. Academic Press, 2021.

[16] R. Hibbeler, *Mechanics of Materials*. Pearson, 2014.